sciendo
Austrian Journal of Earth Sciences | Vienna | 2025 | Volume 118 | 219–240 | DOI: 10.17738/ajes.2025.0013

Sedimentological and pore-scale characterisation of the Bockfließ Formation, Central Vienna Basin: implications for sealing potential

Kanchan Dasgupta[1*], Yaroslav Zechner[2] and Thomas Gumpenberger[1]

[1)] OMV TECH Center Lab, Protteser Strasse 40, 2230 Gänserndorf, Austria
[2)] Geological Archive, Department of Geology, Josef-Holaubek-Platz 2, 1090 Vienna, Austria
[*)] Corresponding author: kanchan.dasgupta@omv.com

Keywords: Bockfließ Formation, facies analysis, MICP, rock strength, sealing potential, sedimentology, Vienna Basin, XRD

Abstract

The Bockfließ Formation represents parts of the Ottnangian Stage of the Lower Miocene in the Central Vienna Basin and is characterized by the type section from the Matzen 269 well. However, a detailed sedimentological characterisation of the type section has not been published. Previous studies on the Bockfließ Formation predominantly focused on fossil assemblages, which indicated a lagoonal depositional environment with riverine input. This study intends to complement previous paleontological studies with a detailed sedimentological analysis, involving lithological, petrographical, ichnological, and macrofossil content descriptions of the cored sections from the Matzen 269 well. The sedimentological data was thereafter used to establish lithofacies and determine depositional environments represented by the cores. This suggests that the Bockfließ Formation in the study area largely represents a coastal lagoon depositional setting, with identified depositional environments include lagoon, washover fan, channel fills (inlet) and shoreface. The lagoon facies is the most dominant and relevant sealing facies in the Bockfließ Formation and could span tens of kilometres at its widest point and most likely formed due to coastal sea flooding. However, a connection was maintained between the lagoon and the sea, representing an inundation model, with modern analogues found in the Venice Lagoon in Mediterranean Sea and the Curonian Lagoon in the Baltic Sea.

The selected core sections were also evaluated for their sealing potential as the formation is a regional caprock for the underlying fractured carbonate reservoirs. The sealing potential of a caprock system depends primarily on its geometry, storage capacity, and structural integrity. To evaluate the sealing potential, lagoon facies were further subjected to XRD, QEMSCAN, MICP and coreDNA analyses. Based on these, the lagoon facies would most likely act as an intraformational seal, given the presence of other non-sealing facies. Rock strength data obtained through scratch testing indicate a subtle variation in strength within the lagoon facies, attributed to clay content. Moreover, the compositional make-up of the lagoon facies is akin to 'sealing shales' reported elsewhere. Additionally, XRD analysis revealed that illite is the dominant clay mineral across the lagoon facies, which is a non-reactive clay mineral.

1. Introduction

The Vienna Basin lies on the pre-Neogene basement, composed of Alpine-Carpathian nappes (Harzhauser et al., 2020; Siedl et al., 2020). The lowest stratigraphic unit of the basin is represented by the Aderklaa Formation, located south of the Matzen/Spannberg Ridge (in the Raggendorf-Matzen-Bockfließ-Schönkirchen areas), while the Badenian units (the Matzen Formation and Baden Formation) are found north of the Matzen/Spannberg Ridge in the Spannberg area. In many areas, the Bockfließ Formation overlies the Upper Triassic Hauptdolomite, which acts as a fractured oil and gas reservoir (Hamilton

et al., 2000; Harzhauser et al., 2020; Siedl et al., 2020; Harzhauser, 2022; Harzhauser et al., 2024a; Harzhauser et al., 2024b). The Bockfließ Formation (Fm), named after the village of Bockfließ, northwest of Vienna, was first described as "brachyhaline Schichten" (brachyhaline beds) based on the Bockfließ 78 well (Papp et al., 1973). Since then, it has been documented in numerous subsurface wells in the area of Spannberg, Prottes, Matzen, Bockfließ, Raggendorf, Schönkirchen, Straßhof, Deutsch-Wagram, Tallesbrunn and Glinzendorf in the Central Vienna Basin. It fills a paleo-relief and is truncated by erosion, hence its thickness varies considerably (Harzhauser et al., 2020).

Previous studies established that the sedimentation of the Bockfließ Fm occurred in a fully marine, lagoonal-coastal depositional environment, with mudflats and soft bottom conditions located in a fully marine environment, and consists lithologically of quartz sands and calcareous clays (Harzhauser et al., 2020). Furthermore, faunistic studies indicate the presence of a riverine inlet, indicating high nutrient availability and salinity variations in the lagoon. Papp et al. (1973) identified macrofossils including marine/brackish gastropods and bivalves such as *Turrtitellids*, *Lucinids* and *Rzehakia* and microfossils including benthic foraminifera *Ammonia beccarii* and *Elphidiinae sp*. In addition, Papp et al. (1973) used *Rzehakia* (*"Oncophora"*) as an index fossil for the Bockfließ Beds (Bockfließer Schichten) and dated the formation of late Ottnangian age. However, recent study by Harzhauser et al. (2020) did not find any occurrence of *Rzehakia* fossils in Matzen and Schönkirchen wells. Furthermore, biostratigraphic significance of the bivalve *Rzehakia* was critically discussed by Schultz (2005), as it has a wide biostratigraphic range from Ottnangian to Badenian and therefore cannot be used as an index fossil (Schultz, 2005; Harzhauser et al., 2020; Ruman et al., 2021). A Recent study by Harzhauser et al. (2020) dated the Bockfließ Fm of an early Ottnangian age based on the nannofossil assemblages comprising nannoplankton zones NN3 and lower NN4.

The Bockfließ Fm is characterized by the type section from the Matzen 269 well (Fig. 1), where a maximum thickness of 500 m has been documented and the base comprises transgressive flysch deposits (Rhenodanubian Flysch) and Mesozoic nappes of the Northern Calcareous Alps (Harzhauser et al., 2020). Furthermore, from the same type section well, approximately 143 meters of drilled core has been recovered, although its detailed sedimentological and pore-scale characterisation has not yet been published. However, several proprietary, unpublished OMV reports exist that describe the sedimentary characteristics of the Bockfließ Fm from the neighbouring wells. Previous published studies focused predominantly on fossil assemblages of the type section, including sampling the cored intervals. This study, therefore, intends to complement previous paleontological studies with a detailed sedimentological analysis of the cored sections from the Matzen 269 well.

The Bockfließ Fm is also known to unconformably

Figure 1: Maps displaying the location of the study area including the approximate position of the type section well of Bockfließ Formation (Matzen 269) in the Central Vienna Basin.

overlie the Pre-Neogene basement and comprises the caprock for fractured reservoirs belonging to the Upper Triassic Hauptdolomite in the Vienna Basin (Hamilton et al., 2000; Sachsenhofer et al., 2024). Hence, the secondary aim of this paper is to assess the implication of the sedimentological and pore-scale results obtained from the current study towards the formation's sealing potential. The sealing potential, as understood in its classical definition by the hydrocarbon exploration industry, combines seal capacity, seal geometry and seal integrity (Surdam, 1997). In general, the capacity is defined by the fluid column height that can physically be held back by the rock; geometry refers to the areal extent and thickness, whilst integrity includes the rock mechanical properties. Additionally, geochemical effects can theoretically increase or decrease caprock's sealing potential (Busch et al., 2016; Worden, 2023).

2. Geological Setting

The Vienna Basin is part of the Neogene Paratethys basin system (Fig. 2), which formed together with the Mediterranean Sea from the vanishing Tethys Ocean approximately at the Eocene/Oligocene boundary (Popov et al., 2004; Harzhauser et al., 2024b). The isolation of the Paratethys was primarily driven by progressive uplift of the Alpine-Carpathian-Dinarid and Balkan Mountain chains, as a result of tectonic movement of Africa towards Eurasia and a rotation of several microplates in the Mediterranean region. Tectonic evolution of the Vienna Basin can be divided into four major stages: (1) Lower Miocene: NW-SE compressional tectonic regime and formation of

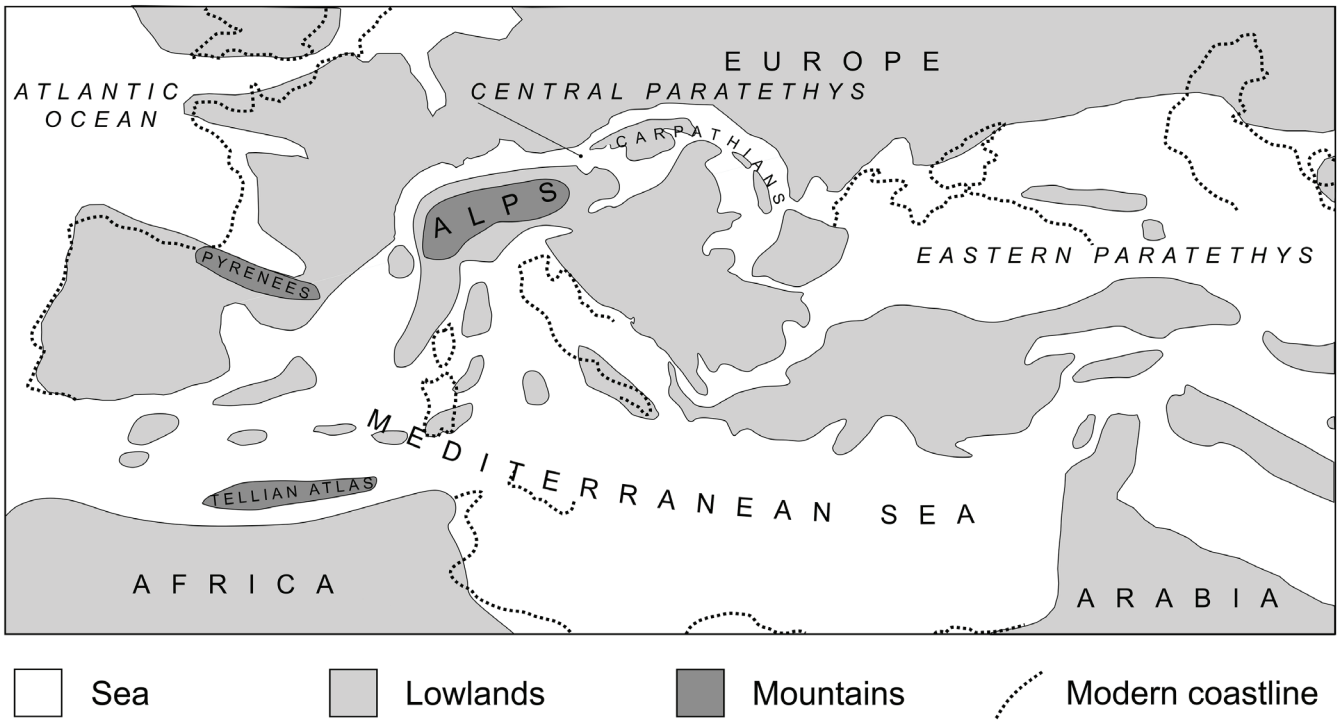

Figure 2: Simplified paleogeographical setting of the study area (after Neubauer et al., 2015).

a piggy-back basin; (2) Middle Miocene: extensional basin; (3) Late Middle Miocene to late Miocene: pull-apart basin, E-W compression and basin inversion; 4) Pleistocene – recent: E-W extrusion (Decker, 1996; Strauss et al., 2006; Hölzel et al., 2010; Siedl et al., 2020; Harzhauser et al., 2024a; Harzhauser et al., 2024b). Deposition of the Bockfließ Fm is associated with the development of the Central Paratethys Sea (Fig. 2) and the evolution of the Vienna Basin (Fig. 3). The following paragraphs outline the important paleogeographical and sedimentological events reported in the published literature during the Early Miocene of the Paratethys Sea and the Vienna Basin developments. It is noteworthy that no rock records are present from the Egerien and Eggenburgian Stages in the Vienna Basin (Harzhauser et al., 2024a).

2.1. Egerian Stage

During Egerian Stage (Late Oligocene - Lower Miocene), the Paratethys was a vast marine sea, oriented west to east. During this period, the Paratethys was connected to the Tethys Ocean in the West, to the North Sea via the Rhine Graben in the North and to the Venetian Basin in the southwest. This teleconnection ceased to exist during the late Egerian. Sedimentation during the Egerian stage was dominated by siliciclastic depositional systems with occurrence of mixed carbonate-siliciclastic systems (Piller et al., 2007).

2.2. Eggenburgian Stage

The Eggenburgian Stage is characterized by shallow marine depositional environments, with predominantly sandy and pelitic near-shore sedimentation. Carbonate systems were rare and had patchy occurrence. Deep neritic to bathyal environments of the Eggenburgian Stage are characterized by grey calcareous clays with intercalations of sands, also called "Schlier" in older literature (Papp et al., 1973). In addition, the western seaway through the Alpine Foreland, which had been sealed during the late Egerian and possibly early Eggenburgian, began to open. The transgression into the foreland occurred successively from the west and entered the Central Paratethys during the late Eggenburgian. In the east, extensive sea connections allowed mollusc faunas to spread to into modern Crimea and Georgia (Kováč et al., 2004; Piller et al., 2007).

2.3. Ottnangian Stage

During the Ottnangian Stage, the paleogeography of the Paratethys resembles similar conditions as during the Eggenburgian Stage. However, in the late Ottnangian tectonic uplift of the Alpine Foreland Basin and global sea level fall severed the western connection to the Mediterranean Sea. Furthermore, geographic differences in the "Rzehakia fauna" between Bavaria, Austria and Moravia suggest that the western Paratethys was disintegrated into several isolated brackish lakes. Sedimentation was predominantly siliciclastic with tidally influenced deposits and occurrence of sandy/silty ("Schlier") sediments. Sedimentation in the Central Vienna Basin commenced during the early Ottnangian Stage and is represented by the Bockfließ and Lužice Fms (Fig. 3) (Harzhauser et al., 2024a).

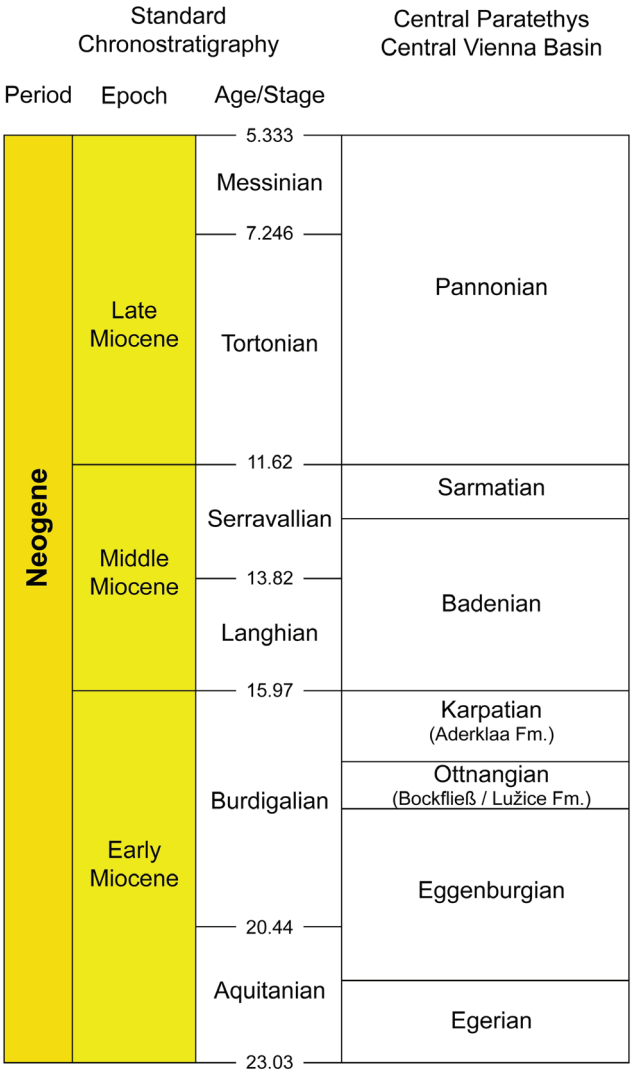

Figure 3: Miocene stratigraphy of the Central Paratethys and Central Vienna Basin (Harzhauser et al., 2024a).

2.4. Karpatian Stage

Tectonic uplift of the Karpatian Stage is characterized by transgression and reorganization of the paleogeographic environment of the Paratethys Sea. In the south, a new broad connection with the Mediterranean via the "Trans-Tethyan Trench Corridor" was established. The newly established seaway, led to an extensive faunal exchange between the Central Paratethys and the Mediterranean Seas. However, the connection with the Eastern Paratethys ceased its existence due to tectonic uplift of Carpathian Mountain System. In the Central Vienna Basin, the Stage is represented by the Aderklaa Fm (Fig. 3), which consists of lower member (Gänserndorf) and upper member (Schönkirchen) (Harzhauser et al., 2020).

The Gänserndorf Member represents a transition from alluvial fans to a braided river system, with main flow direction from SW to NE. In addition, several sections of the member represent overbank-deposits and possibly wetland ponds. Furthermore, paleosols and anhydrite pebbles were reported, indicating terrestrial and dry climatic conditions. The Gänserndorf Member discordantly overlies the Bockfließ Fm, with alternating conglomerates, sandstones, marly silty clays and breccias (Harzhauser et al., 2020). The Schönkirchen Member resembles strongly cemented sandstones with marly silts and marly clays, intercalated with thin gravel layers, representing meandering river system with channels and flood plains.

3. Methodology

3.1. Core logging

The cores, principally unslabbed and whole in nature, were described at the core storage facility of OMV in Gänserndorf, Austria through visual analysis of lithologies, grain size variations, sedimentary structures, bioturbation intensity, body and trace fossils plus cementation. Subsequently, the collected data was documented as a log at a 1:50 scale and digitized using EasyCore software. Particular attention was paid to the ichnology of the succession and the bioturbation scheme applied here is after (MacEachern et al., 2012). All cores were also photographed under natural light conditions as high-resolution images.

The sedimentological logging workflow utilised a bed/sub-bed scale lithofacies scheme, based on primary texture, lithology, sedimentary structures, bioturbation, and, where relevant, any additional lithological and/or diagenetic features such as clasts, carbonaceous matter, and cementation. These lithofacies do not have direct environmental implications but provide the building blocks for sedimentary process interpretation. The lithofacies have been further grouped into bedset to bedset stack-scale for obtaining genetically related facies which are likely related to the environment of deposition. The interpretation of facies or depositional elements is based on the nature, stacking patterns, depositional context and relative occurrence of lithofacies. Additionally, the intensity and diversity of trace fossil assemblages, presence of macrofossil and microfossil assemblages, play an important role in the interpretation of the depositional environment.

3.2. Petrography

Standard petrographical techniques were used throughout the thin-section analysis program. All thin-section samples were vacuum impregnated with blue-dyed epoxy resin to enable the characterization of the pore spaces. Thin-sections were also stained for carbonates with combined alizarin red-S and potassium ferricyanide to facilitate the identification of the carbonate mineralogy (Dickson, 1965). Terms used for routine thin-section descriptions under microscope as well as report sections (eg. poor, good) are quantified in the following way: dominant >15 %; subordinate 5–15 %; minor 1–5 %; rare <1 %.

In addition, a subset of the samples underwent QEM-

SCAN analysis (Quantitative Evaluation of Minerals by Scanning Electron Microscopy) at Viridien, UK using a Quanta 650F automated mineralogy system. This comprises a scanning electron microscope with energy dispersive spectrometers (EDS), microanalyser and an electronic processing unit, integrating the scanned data to provide information about the 2D textural and mineralogical composition of each sample. The scanning resolution for all samples is 10 µm and are all conducted at a standardized electron beam voltage of 15 keV, with the analysis focusing on a 10x10 mm representative area of the sample.

3.3. Mineralogy

Routine petrography analysis provided the gross mineralogical composition of the studied formation. However, selected core samples were also subjected to X-Ray diffraction analysis (XRD) for quantifying and corroborating the mineralogical composition. The bulk mineralogical composition was determined on powdered samples using a Bruker AXS D8 Advance X-ray diffraction spectrometer (copper radiation generated at 40 kV and 40 mA). Subsequently, the software program DIFRAC. EVA V3 was used for the identification of different mineral phases. Quantification of minerals detected by XRD is based on peak heights within the spectrum based on the method after (Schultz, 1964) and internal standards. Based on comparison with other methods and other laboratories, the quantification results show an absolute error range of 2–5 %.

Clay minerals were evident in whole-rock diffractograms. However, in order to better identify the clay minerals, the clay fraction (<2 µm) was extracted and analysed separately. Organic material was removed using H_2O_2 and the samples were dispersed using an ultra-sonic cleaner. The grain fraction <2 µm was separated by using the Atterberg method (separation of particles with certain size and density in a water-filled cylinder based on Stoke's law). The <2 µm fraction was thereafter pressed on corundum pads by a water pump-jet and placed on the sample holder for XRD analysis. Consequently, two measurements were performed to identify swelling clays before and after the saturation of the sample with ethylene glycol.

3.4. Mercury Injection Capillary Pressure (MICP)

Capillary curves and pore throat radii distributions were obtained by mercury injection using a fully automated system (Autopore V from Micromeritics). Samples were irregularly shaped, and weight was typically between 8 and 15 g. Furthermore, when possible, pieces were taken from the end trims of core plugs. The investigated pressures range from 0.0001 to 4133 bar with 100 % of pore volume saturation assumed at 4133 bar. Prior to the start of mercury injection, the samples were evacuated to a pressure equivalent to 0.2 mbar, with an additional evacuation time of 5 min. Equilibration time between two pressure stages was 90 s. Additionally, the instrument was set up in such a way that if the intrusion exceeds 0.001 ml/s per gram of sample, an additional equilibration point is added, in order to better resolve the capillary pressure-curve (pc-curve). Closure corrections and the calculation of capillary entry pressure (pd) were based on the methods described by Thomeer and Murphy (2000).

3.5. CoreDNA

A subset of the core samples were also subjected to CoreDNA testing (EPSLOG©) that combines a suite of analyses to produce a transdisciplinary, high-resolution dataset (Germay et al., 2023). Given the historical nature of the cores, optimal core orientation was ensured from sedimentological descriptions. The cores were thereafter scanned along a fit-for-purpose surface with a collection of sensors. The flat, horizontal surface was created by successive dry cuts with a square polycrystalline diamond compound blade. Each dry cut removes a sub-mm thick rock layer. All CoreDNA sensors were deployed on the same groove created by the blade.

The generated dataset included ultra-high-resolution photographs, portable XRF measurements, laser scan, probe permeability, P- and S-wave velocity log and scratch test data. Panoramic photographs were processed to extract textural and colour features, as well as grain size distributions. These findings were supported by analyses of topographical maps created with laser scans (Germay et al., 2023). In this study, particular focus was given to the continuous profiles of elements obtained from the portable XRF system and rock strength from the scratch tests. Details on the scratch tests can be found in Germay et al. (2023) and Richard et al. (2012).

4. Results and interpretations

4.1. Sedimentology

The analyzed cores cover approximately 143 meters of the Bockfließ Fm in the Matzen 269 well (Fig. 4). However, a maximum formation thickness of about 500 meters has been documented in this well (Harzhauser et al., 2020). The cores were primarily cut from the top and bottom hundred metres of the succession (Fig. 4). Furthermore, the cores include the following lithologies, in order of their decreasing relative abundance: siltstones, sandstones, calcareous mudrocks (marlstones), and both mud-prone and sand-prone heterolithics. A total of 66 lithofacies were identified to characterise the cores in high resolution. However, during data analysis these lithofacies were grouped together for the interpretation of facies. The following facies have been assigned to the cored intervals (Fig. 4): lagoon (46 %), washover fan (24 %), shoreface (16 %), channel fills (10 %) and channel margin (4 %). Each of the facies characteristics are described below and illustrated in Figures 5–10. Additionally, the

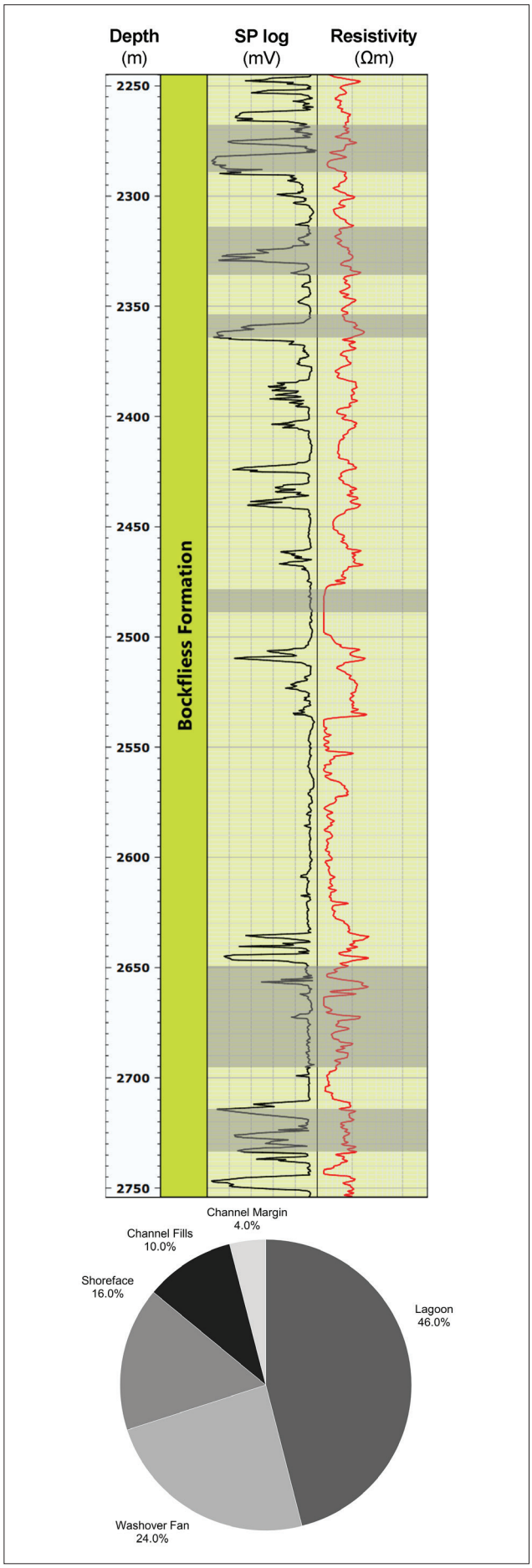

characteristics of the grouped lithofacies are summarised in (Tab. 1).

4.1.1. Lagoon

Description: The most common facies within the cored interval is the lagoon facies, predominantly represented by siltstones and minor amounts of calcareous mudrocks and mud-prone heterolithics (Figs. 5 and 6). Sandstones occur rarely with sharp tops and bases with grain sizes ranging up to fine sand. All of the lithologies are typically bioturbated with variable intensity (weak to moderate), locally carbonaceous and are laminated to massive. Lamination is in general low-angle and planar although rare rippled-lamination, convolute lamination and slump structures are noted among sandstones and heterolithic beds. Broken shells of bivalves and gastropods commonly occur among all the lithofacies except for sandstones. Gastropods are represented by *Terebralia sp.* Moreover, Harzhauser et al (2020) identified bivalves such as *Nuculana sp.*, *Ostrea digitalina*, *Papillicardium papillosum*, *Corbula gibba*, and *Macoma elliptica* from Matzen 269 deposits (Harzhauser et al., 2020). Trace fossil assemblage is composed of following ichnofossils: *Planolites, Teichichnus, Thalassinoides, Scolicia, Palaeophycus, Phycosiphon* and *Schaubcylindrichnus freyi* (Figs. 5 and 6).

Siltstones and calcareous mudrocks typically display laminated fabric at the microscopic scale. The mm-cm lamination is continuous to broken in nature. Moreover, horizontal mm-scale burrows were observed in thin-section, representing *Palaeophycus* and *Phycosiphon* trace fossils. Such burrows are enriched with silt-sized detrital minerals such as quartz and feldspars. QEMSCAN analysis further indicated that locally these burrows are cemented preferentially with dolomite and calcite. Conispirally coiled foraminifera (rotaliids) tests occur rarely within calcareous mudrocks and siltstones (Fig. 6).

Interpretation: The lithofacies make-up, comprising predominantly mud and silt, points to a low energy depositional setting. Furthermore, physical sedimentary structures suggest slow rates of terrigenous sediment influx with a complete absence of tidal influence. Bioturbation is extensive and comprises shallow-tier trace fossil assemblage. The trace fossil assemblage suggests brackish-water conditions (Knaust and Bromley, 2012). Moreover, the lagoon facies sediments contain mudflat gastropods and the bivalve *Corbula gibba*, which can withstand dysoxic and instable bottom conditions. The small size of these stress-adapted infaunal species further indicates a dysoxic and highly stressed marine environment (Talman and Keough, 2001).

Figure 4: Vertical distribution of the available subsurface cores from the type section of Bockfließ Fm in well Matzen 269. The cores, highlighted in grey shading, cover only c.28 % of the entire formation in this location. Left wireline log is SP log whilst the right one is deep resistivity log. Pie chart indicates the distribution of facies among the logged core.

Table 1: Lithofacies characteristics from the cored intervals of Bockfließ Formation in Matzen 269 well.

Code	Lithofacies	Description	Sedimentary processes
Sim	Massive siltstone	Structureless grey- coloured siltstone. Carbonaceous material and various degree of bioturbation are common. Locally, fractured as well as clast-charged (granular and pebbly). Occasionally with fossils of bivalves, gastropods and brachiopods.	Deposition from high-viscosity sediment–water flows under low-energy conditions or in standing bodies of water (mudflows)
Sil	Laminated siltstone	Grey-coloured horizontally-laminated siltstone, locally discontinuous. Often contains carbonaceous detritus and in general moderately bioturbated, with an average bioturbation index of 3. Locally fractured (70 - 100°).	Deposition from suspension settling of clay and silt-grade sediment in very-low-energy conditions.
Sm	Massive sandstone	Structureless grey-, buff-coloured, very fine- to fine-grained sandstone. Rounded to subrounded, well- to moderately sorted quartz grains, locally with glauconite. Carbonaceous material and various degree of bioturbation are common. 0.1–4 cm diameter mud clasts often present along with sharp basal contacts. Usually occurs with no signs of bioturbation and fossils.	Rapid deposition from high- density sediment gravity flow deposits and/or post-depositional modification. Mudstone rip-up clasts from the underlying bed.
Sl	Laminated sandstone	Buff-coloured, well-sorted, rounded to subrounded grains typically of quartz, parallel-laminated sandstone, locally angle planar lamination. Dominantly very fine- to fine grained sandstone. Carbonaceous material and various degree of bioturbation are common, locally with 0.1–3 cm diameter.	Planar bed flow under lower and upper (flash flood) flow regimes. Parallel lamination in very-fine- to fine-grained sandstone can be deposited from suspension, slow-moving sediment clouds/ low-density turbidity currents
Shcs	Hummocky cross-stratified sandstone	Grey- to buff-coloured, very-fine- to fine-grained, carbonaceous, hummocky cross-stratified sandstone. Poorly to occasionally bioturbated. Also present within interbedded intervals (heterolithic units).	Represents deposition during high-energy oscillatory or combined flows (waves and currents) under storm wave conditions (below fair-weather wave base).
Sx	Cross-bedded sandstone	Light-grey- to buff-coloured, very fine to fine-grained sandstone usually well sorted, carbonaceous with rounded to subrounded quartz grains. Mudclast-charged locally, max 3cm in diameter. Tabular cross-bedding with individual foreset angles ranging between 10 to 40°. Individual cross-beds range in thickness from 0.5 to 8 cm and often show a fining-upwards trend within each foreset laminae.	Unidirectional migration of 2D straight-crested dunes and thalweg bars in high-energy fluvial channels, under lower flow regime
Sd	Deformed/ convolute laminated sandstone	Contorted and overturned laminae in very-fine- to fine-grained, grey- to buff-coloured, well-sorted sandstone. Also present within very-fine sandstones of heterolithic intervals.	Post-depositional slumping and soft-sediment deformation associated with channel-bank collapse, dewatering processes as a result of rapid deposition and/or shearing of the sediment surface by currents
Sr	Ripple cross-laminated sandstone	Buff-coloured, fine-grained sandstone with asymmetrical unidirectional ripple laminations. Very- well- to moderately sorted sandstone and associated with heterolithics.	Mutually erosive ripples represent migration of ripples with a low–moderate rate of sedimentation.
cMm	Massive marlstone	Structureless grey- to black-coloured marlstone. Usually contain carbonaceous material and various degree of bioturbation. Locally graded, with occasional occurence of shell remains.	Deposition from high-viscosity sediment–water flows under low-energy conditions or in standing bodies of water (mudflows). Graded bedding reflects changes in flow conditions during sedimentation
cMl	Horizontally laminated marlstone	Similar to cMm but with faint to distinct lamination.	Deposition from suspension settling of clay and silt-grade sediment in very-low-energy conditions.
mH	Laminated, mud-prone heterolithic	Dark-grey- to black-coloured, thinly interbedded mudstone and siltstone. Often carbonaceous and moderately bioturbated with planar to wavy-laminated siltstone. Streaky sandstone laminae with small-scale ripples including climbing ripples and broken lenticular bedding. HCS in some sandstone beds/lenses. Rare syneresis cracks. Individual sandstone/mudstone beds typically range from 2 to 70 cm thick.	Climbing ripples are formed during ripple migration under high suspended sedimentation rates. Lenticular bedding is formed by suspended mud in the water depositing on top of small formations of sand once the water's velocity has reached zero. Syneresis cracks are traditionally ascribed to subaqueous shrinkage whereby salinity changes caused deflocculation of clay.
sH	Laminated, sand-prone heterolithic	Similar to mHl but here sandstone represents the bulk of the interbedded units. Locally, deformed/convolute laminated sandstone also present within this unit.	

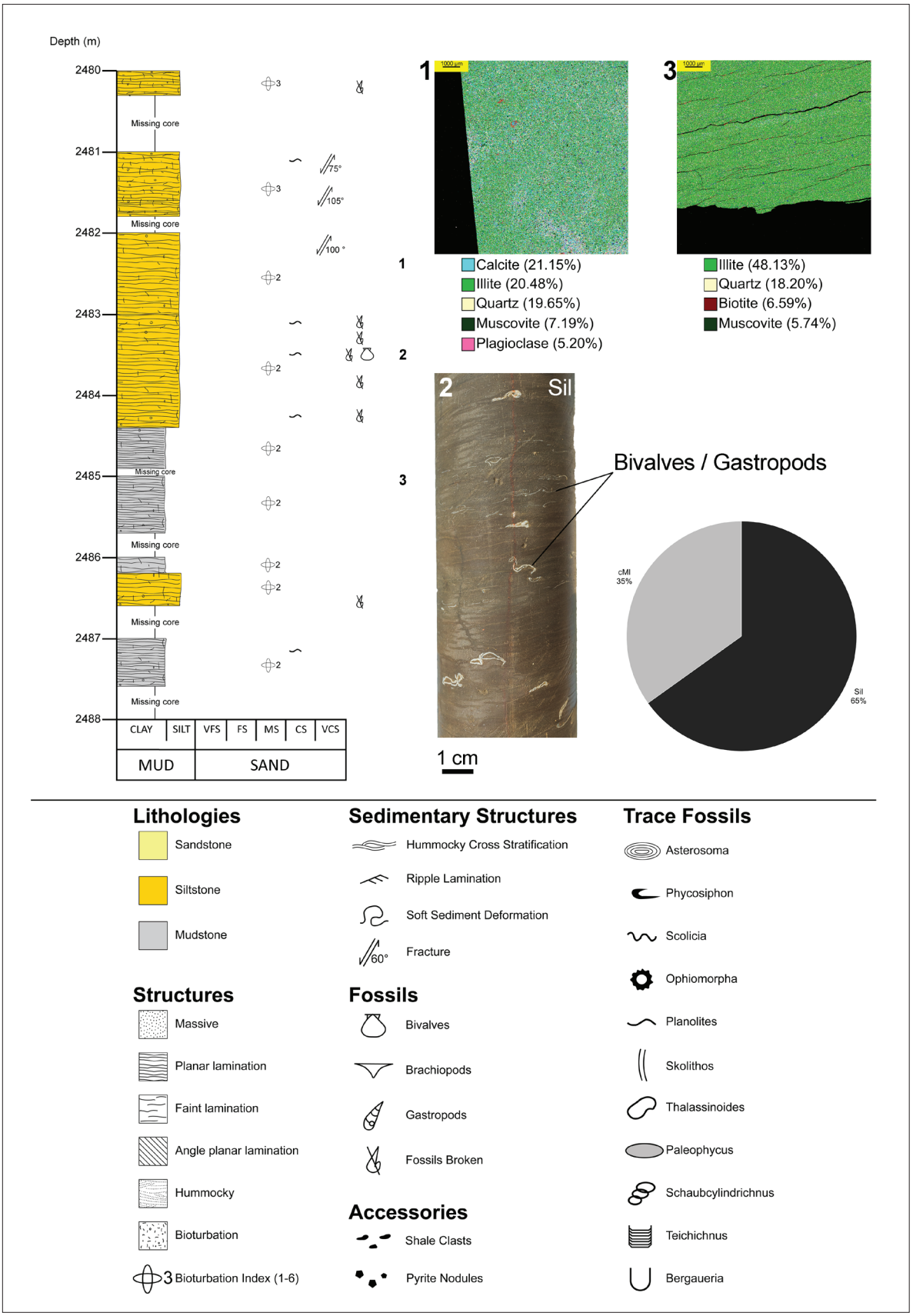

Figure 5: Legend for sedimentary logs and key characteristics of deeper Lagoon facies in Matzen 269 well, including graphic log, QEMSCAN photomicrographs and constituent lithofacies make-up as pie chart. Numbers relate the whole core photographs and QEMSCAN photomicrographs to their position within the displayed cored interval. QEMSCAN photomicrographs correspond to depths of 2482.45 m and 2485.15 m for 1 and 3 respectively, with the legends highlighting minerals >5 % relative abundance. For lithofacies description, see Table 1.

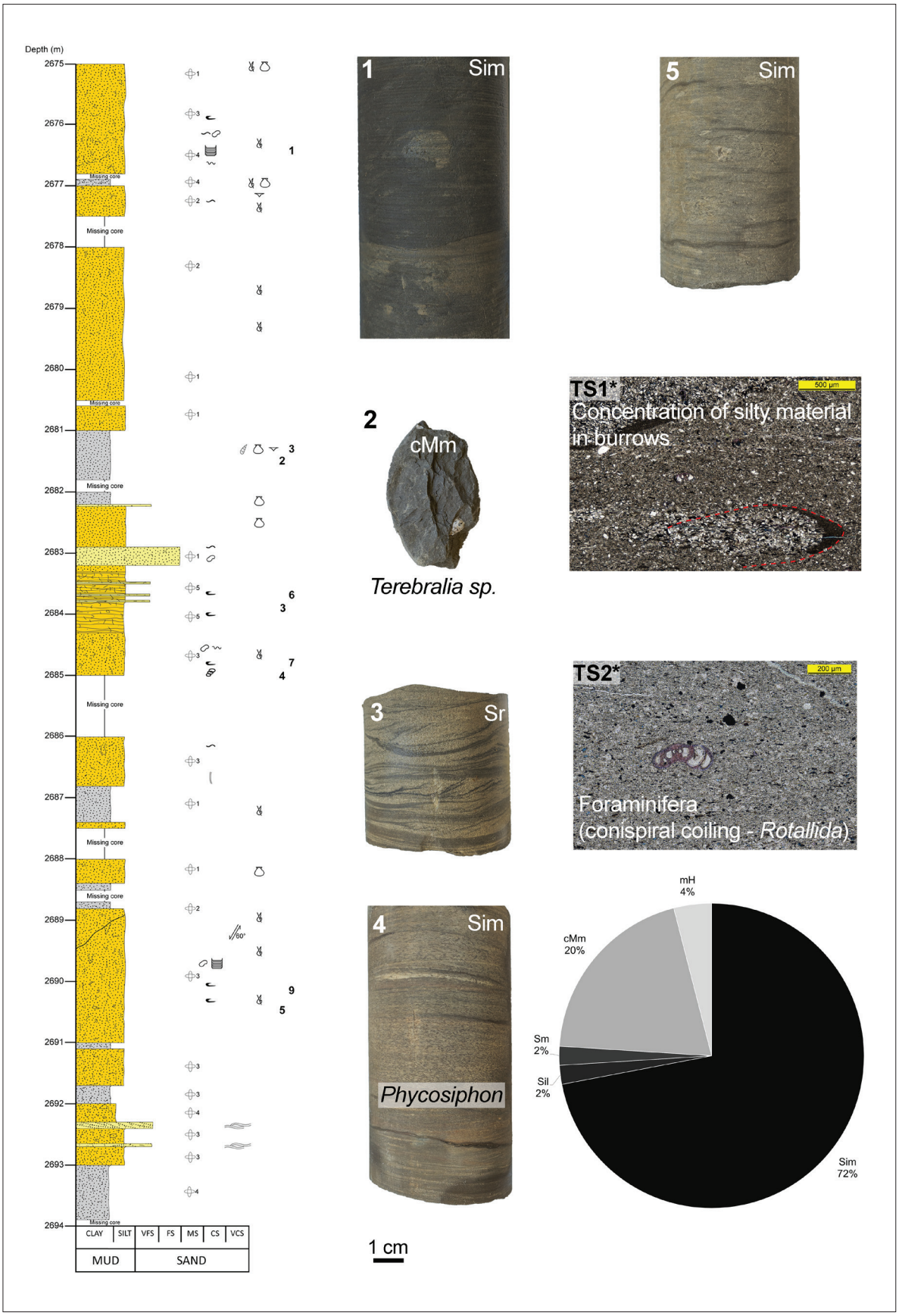

Figure 6: Key characteristics of shallower Lagoon facies in Matzen 269 well including graphic log, thin-section photomicrographs and constituent lithofacies make-up as pie chart. Numbers relate the whole core photographs to their position within the displayed cored interval. Thin-section photomicrographs (TS1* at 2652.62 m and TS2* at 2664.35 m) are from intervals not displayed here. For lithofacies description, see Table 1.

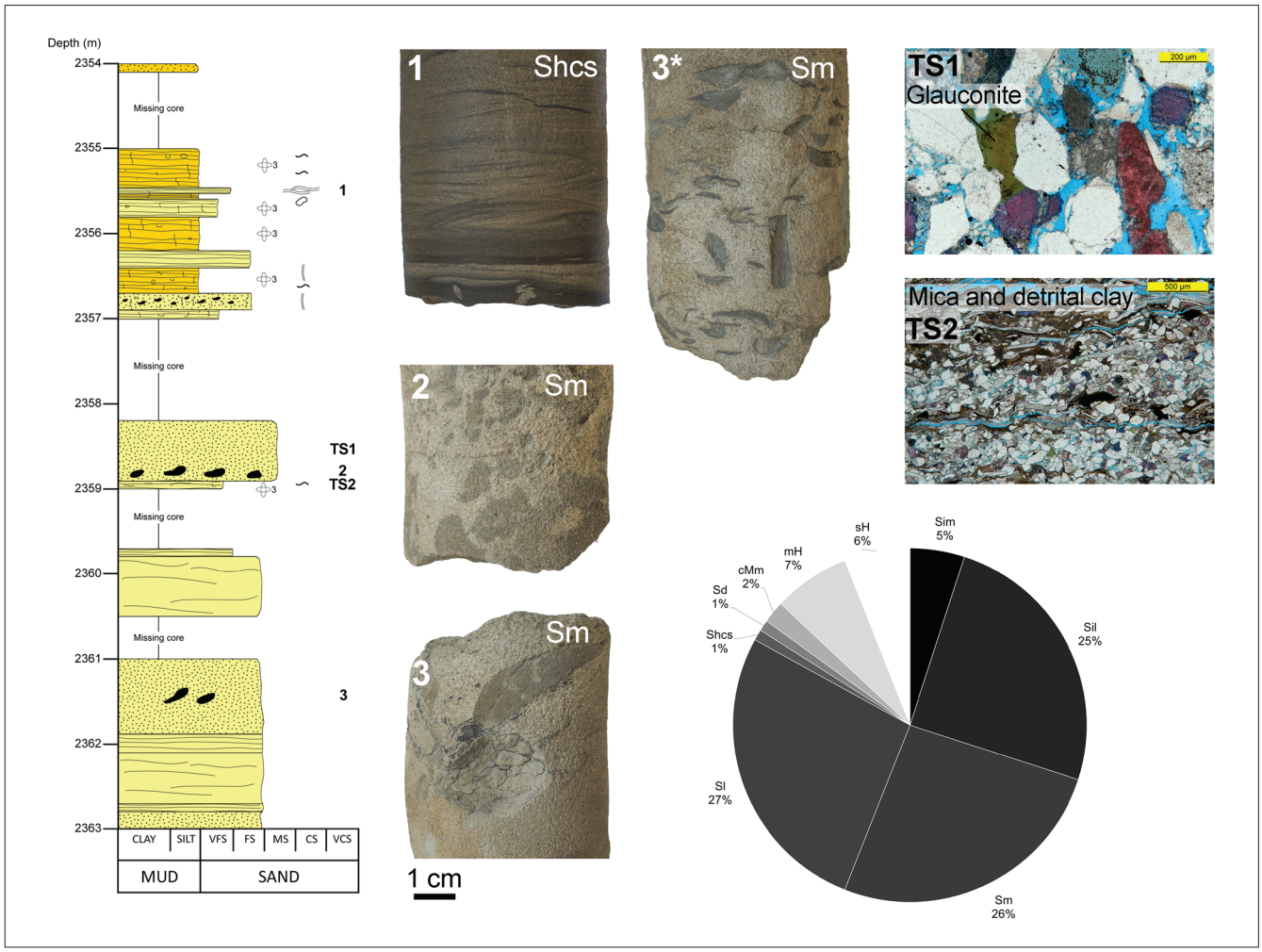

Figure 7: Key characteristics of Washover Fan facies in Matzen 269 well including graphic log, thin-section photomicrographs and constituent lithofacies make-up as pie chart. Numbers relate the whole core photographs to their position within the displayed cored interval (except for 3* whose position is not shown here). Thin-section photomicrographs were sampled at 2358.57 m for TS1 and 2359.07 m for TS2 respectively. For lithofacies description, see Table 1.

4.1.2. Washover Fan

Description: The washover fan facies is predominantly composed of fine-grained, well-sorted sandstones (Fig. 7). These sandstones are massive to laminated, carbonaceous, occasionally bioturbated, displaying rare coarsening-upwards trend as well as soft-sediment deformation. Locally, sandstones contain subrounded mudclasts (up to 4 cm long) and hummocky cross-stratification. Additionaly, a 80 cm thick, massive, medium-grained sandstone unit with glauconite was noted at 2358.2–2359 m (Fig. 7), which was not documented elsewhere amongst the analysed core. Other lithofacies include calcareous, massive to laminated mudrocks, siltstones and mud-prone heterolithics. The latter two lithofacies locally contain carbonaceous detritus and trace fossils such as *Planolites* and *Thalassinoides*.

Under the optical microscope, the sandstones appear structureless to laminated (ripple), defined by oriented mica grains and concentration of detrital clays (dominantly illite). The framework grains typically comprise subrounded quartz and feldspars (primarily plagioclase). Ductile minerals include muscovite, biotite and glauconite, whilst carbonate phases such as dolomite, calcite and siderite make up the authigenic suite. Locally, the sandstones are relatively porous, with primary intergranular porosity being the typical pore type.

Interpretation: The sandstone units, given their stratigraphical position, appear to represent high-energy events within otherwise periods of low sedimentation. The occurrence of interbedded sandstones with hummocky and swaley cross-stratifications suggests a phase of vigorous activity, which eventually subsided into lower energy. Variations in the energy regime probably represent a storm activity. Moreover, presence of hummocky cross stratification within sandstone-siltstone intervals indicates storm influence in the middle-lower shoreface settings, typically situated above the storm wave base (Morsilli and Pomar, 2012; Reineck and Singh, 1973). Furthermore, the unusual occurrence of the thin sandstone unit with glauconite suggests reworked sedimentation,

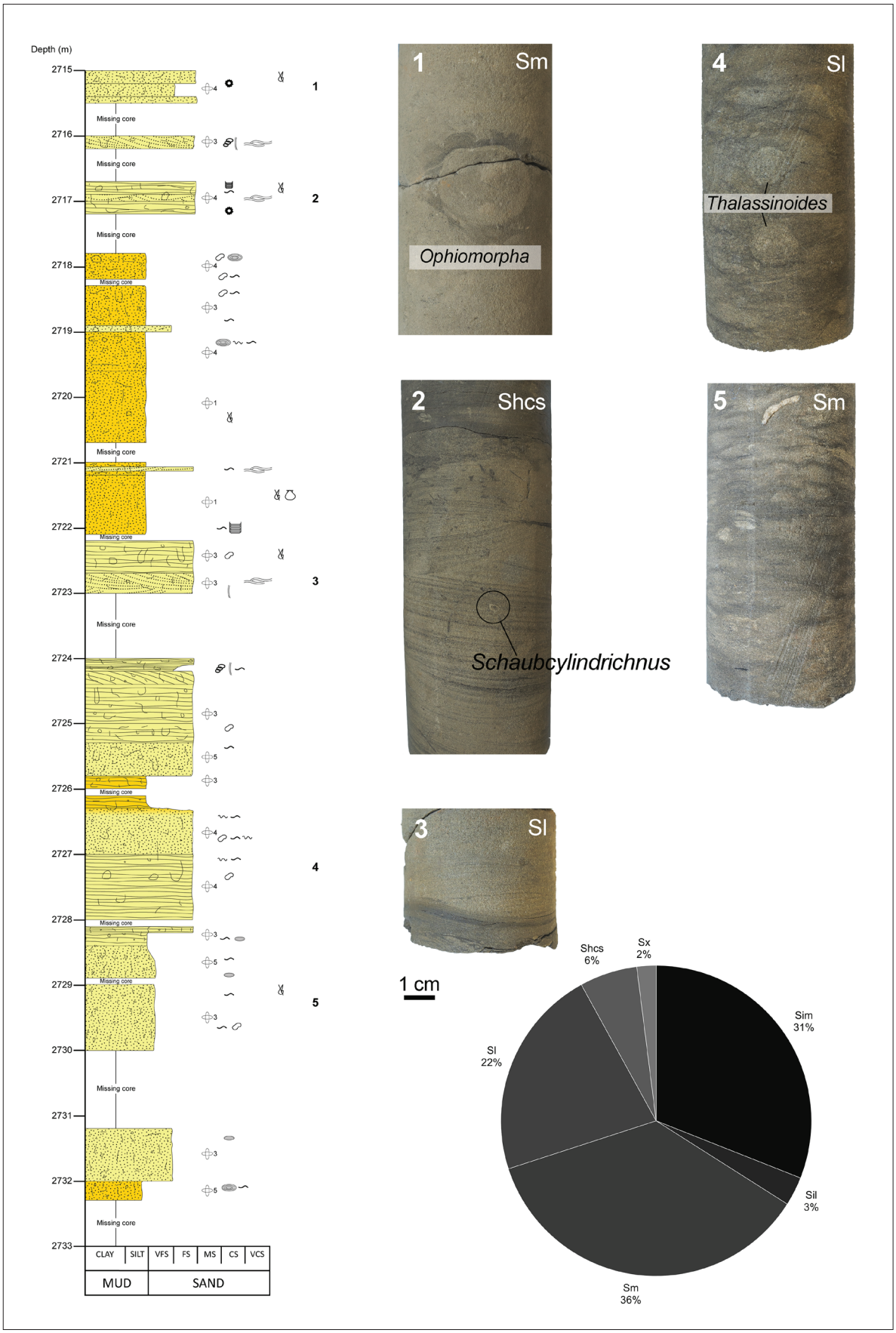

Figure 8: Key characteristics of Shoreface facies in Matzen 269 well including graphic log and constituent lithofacies make-up as pie chart. Numbers relate the whole core photographs to their position within the displayed cored interval. For lithofacies description, see Table 1.

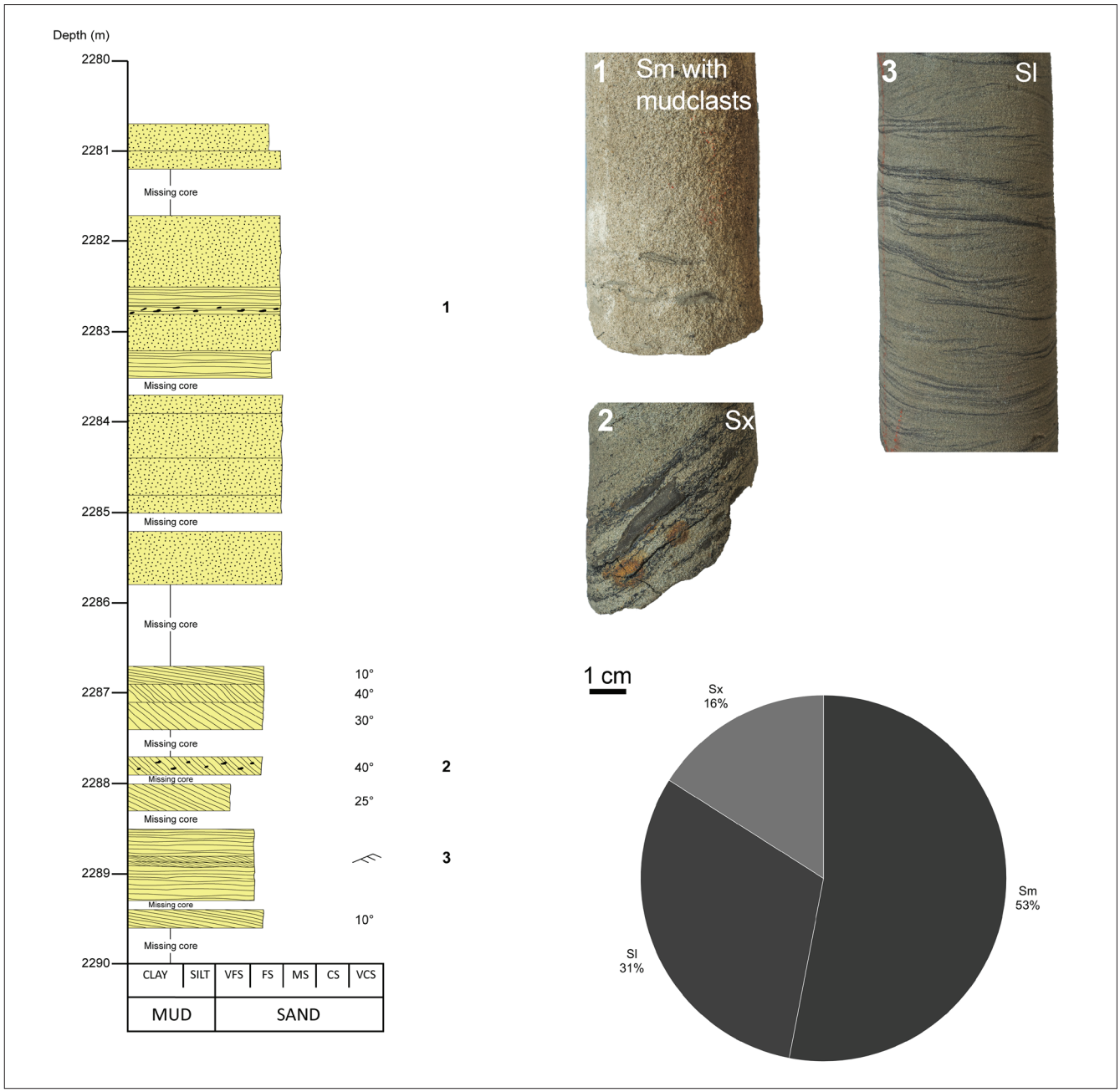

Figure 9: Key characteristics of Channel Fills in Matzen 269 well including graphic log and constituent lithofacies make-up as pie chart. Numbers relate the whole core photographs to their position within the displayed cored interval. For lithofacies description, see Table 1.

given that glauconite typically forms gradually in shallow marine settings with low sedimentation rates and indicates an overall quiet water paleoenvironment of deposition (McRae, 1972; Rubio and Lopez-Perez, 2024). However, the sedimentation rate in the Central Vienna Basin during Ottnangian was high, at least 1 m/kyr (Harzhauser et al., 2020), suggesting that the glauconite-bearing sediments were possibly reworked during transgression and resedimented as part of the of the washover fan during possible storm surges that may have breached a barrier separating the lagoon from the open marine environment.

4.1.3. Shoreface

Description: Sediments from this facies (Fig. 8) occur only in the bottommost part of the core, which cover the interval between 2715 and 2733 m depth with a total thickness of 18 m (Fig. 4). Bioturbated sandstones are common within the facies, with subordinate amounts of siltstone and rare occurrence of mud-prone heterolithics. The sandstones are well sorted, fine grained, typically displaying laminated structures with wedge-shaped sets of parallel laminae. Furthermore, hummocky and high-angle cross stratifications occasionally occur. The siltstones are typically massive and sandstone beds fine upwards gradually to siltstone (Fig. 8). Carbonaceous de-

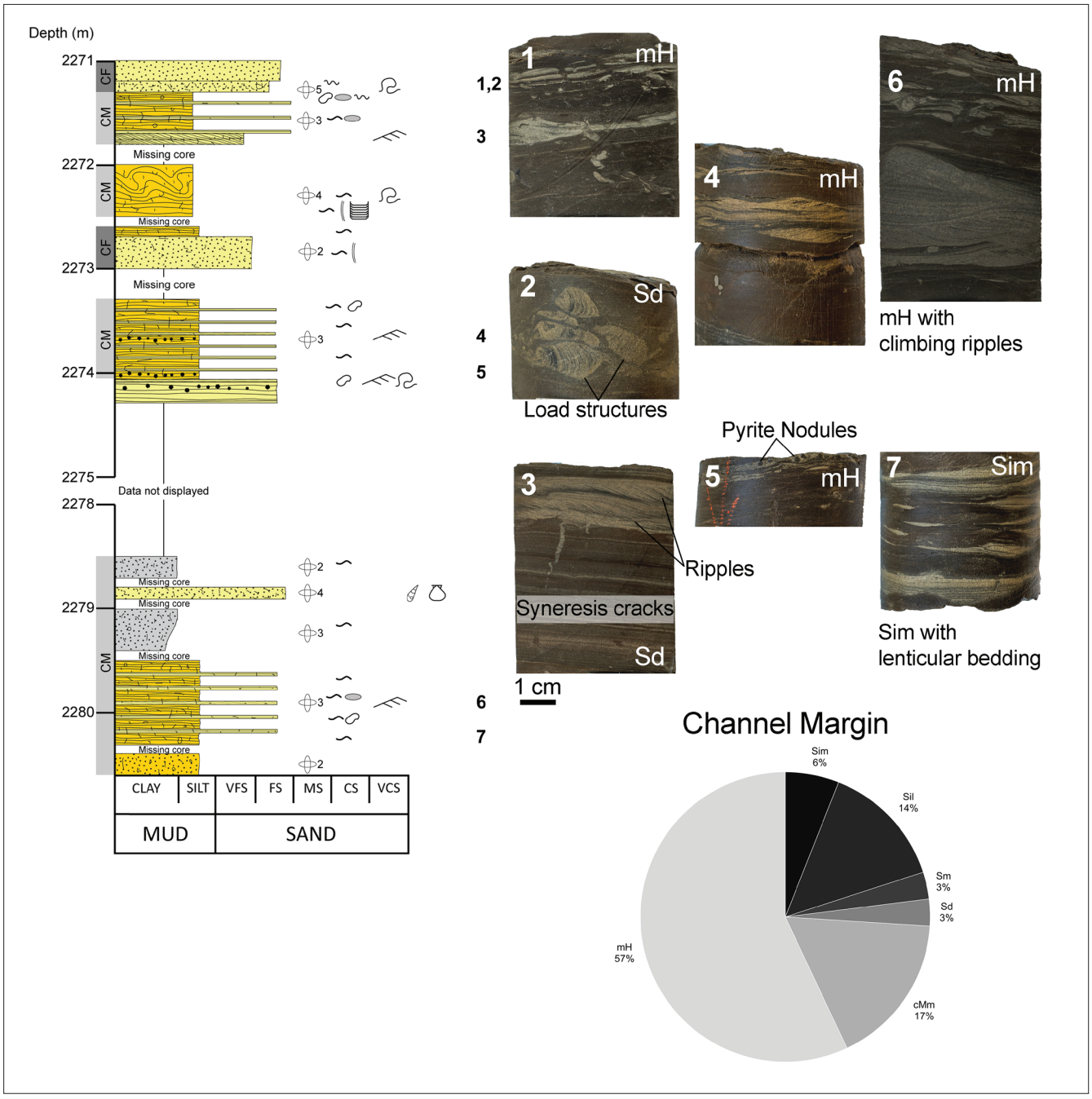

Figure 10: Key characteristics of Channel Margin facies in Matzen 269 well including graphic log and constituent lithofacies make-up as pie chart. Numbers relate the whole core photographs to their position within the displayed cored interval. For lithofacies description, see Table 1.

tritus is common in this facies association with localised occurrence of bioclasts. The ichnological assemblage includes trace fossils *Ophiomorpha*, *Asterosoma*, *Planolites*, *Teichichnus*, *Thalassinoides*, *Scolicia*, *Skolithos, Schaubcylindrichnus* and *Chondrites* (Fig. 8).

Interpretation: The sandstone beds are well-sorted, with physical structures primarily consisting of low-angle, wedge-shaped sets of parallel laminae, along with some hummocky cross-stratification. These features suggest that the sediments were deposited in a wave dominated environment. Furthermore, the presence of *Asterosoma* hints at marine conditions. The trace fossil assemblage indicates a dominance of suspension-feeding organisms over deposit-feeding ethologies. Based on sedimentological and lithological features, along with the trace fossil assemblage consisting of *Skolithos, Ophiomorpha, Schaubcylindrichnus* and *Palaeophycus*, the interval represents middle shoreface facies (Pemberton et al., 2012).

4.1.4. Channel Fills

Description: This facies is composed of 2 to 10 m-thick sandstone intervals, which often display fining-upwards

trends comprising 10 cm-1 m thick sandstone unit with sharp or erosive bases (Fig. 9). They are commonly buff-coloured and visually comprise well to moderately sorted, subrounded to rounded quartz grains. Individual units contain fining-upwards, fine-grained, planar to cross-bedded sandstones. Lamination is defined with wispy carbonaceous and argillaceous material. Furthermore, the apparent dips of cross-bedding foresets measure between 25° and 40° (Fig. 9). In addition, structureless sandstones are also present, locally with rip-up mudclasts up to 3 cm in diameter. Bioturbation is absent (Fig. 9).

Interpretation: Cross-bedded sandstones and sharp-based erosional surfaces represent high-energy erosion and deposition by channels (Tucker and Jones, 2023). Moreover, pebble lags above erosive surfaces indicate rapid deposition of poorly sorted bedload (Reineck and Singh, 1973). Mudstone/carbonaceous drapes along the foresets were probably formed because of slack water periods associated with tidal processes. However, distinct tidal bundles, reactivation surfaces or bi-directional foresets are lacking. Single ≥2 m-thick fining-upwards units likely represent individual channel fills. However, the stacked units, which lack mudstone interbeds, represent amalgamated channel bars deposited possibly as a result of vertical aggradation and lateral migration (Allen, 1983; Bridge, 2006; Miall, 2006).

4.1.5. Channel Margin

Description: The channel margin facies is characterized by mud-prone heterolithics, which have overall minor relative abundance in the studied cores (Fig. 10). Furthermore, structureless calcareous mudrocks, laminated and massive siltstones, sand-prone heterolithics, and rare sandstones

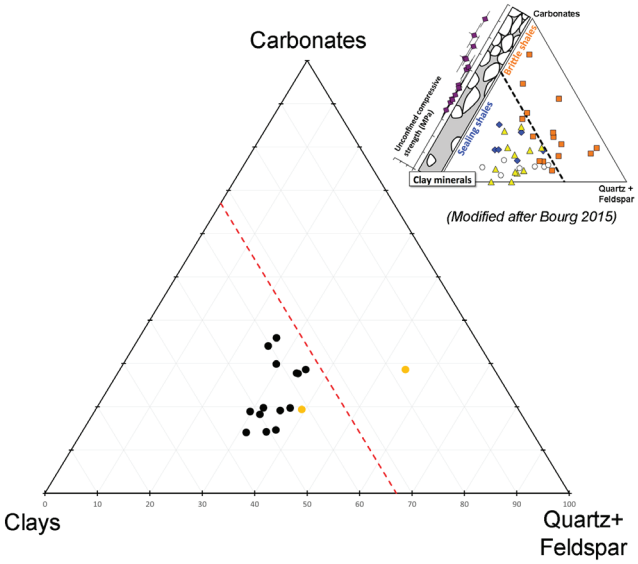

Figure 11: Ternary diagram of the whole-rock XRD analysis of selected samples from the cored intervals of Bockfließ Formation in Matzen 269 well. Black dots indicate lagoon facies, whereas yellow dots represent Washover Fan facies. Dashed line represents the 33 %-clay threshold after Bourg (2015).

characterize the facies (Fig. 10). The heterolithics contain carbonaceous detritus and display parallel lamination with occasional bioturbation. Moreover, rare evidence of climbing ripples, lenticular bedding and syneresis cracks were also observed within the heterolithic sequences (Fig. 10). The mudrocks are locally graded, whilst the sandstones are very fine to fine-grained, massive to laminated, carbonaceous and occasionally bioturbated. Siltstones are laminated and occasionally bioturbated. This facies association is also characterised by fining upwards to trendless

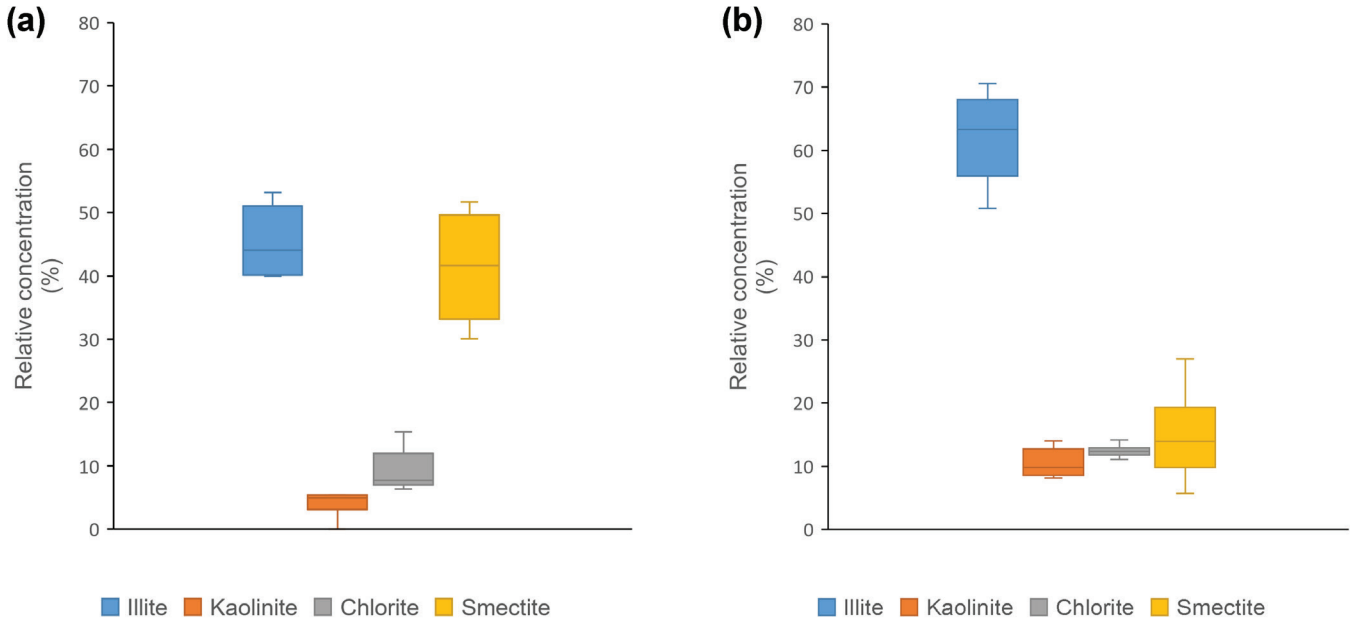

Figure 12: Clay mineral contents of lagoon facies: **(a)** shallower (Cf. Fig. 6); **(b)** deeper (Cf. Fig. 5).

Depth (m)	Lithofacies	Facies	Illite (%)	Kaolinite (%)	Chlorite (%)	Smectite (%)
2481.21	Sil	Lagoon (shallow)	53.2	5.4	7.3	34.2
2482.45	Sil		42.8	5.4	7.2	44.5
2483.00	Sil		40.1	0.0	8.2	51.7
2484.18	Sil		45.3	5.0	10.8	38.8
2485.15	cMl		50.3	4.2	15.4	30.1
2487.16	cMl		39.9	4.8	6.3	48.9
2650.38	cMl	Lagoon (deep)	67.8	9.2	11.1	11.9
2651.75	Sim		62.5	9.2	13.0	15.3
2651.92	cMm		50.8	10.4	11.8	27.0
2652.62	Sim		70.6	8.4	11.9	9.1
2653.45	Sim		64.1	10.7	12.6	12.6
2654.24	Sim		68.1	13.4	12.8	5.7
2664.35	cMl		59.6	8.2	12.1	20.1
2664.40	mH		54.7	14.0	14.2	17.1
2655.60	Shcs	Washover Fan	64.6	23.3	12.1	-
2657.88	Sim		69.7	13.9	14.3	2.1

Table 2: Clay mineralogy data obtained from XRD analysis (clay-fraction).

Depth (m)	Lithofacies	Facies	Pore throat mode (µm)	Pore throat D50 (µm)	ϕ_{Hg} (%)	$k_{Thomeer}$ (nD)
2333.40	Sm	Washover Fan	1.2968	0.8445	12.08	1.983
2334.10	mH		0.0221	0.0221	5.87	0.001
2481.21	Sil	Lagoon	0.0078	0.0070	7.07	0.036
2482.45	Sil		0.0078	0.0071	7.22	0.037
2483.00	Sil		0.0110	0.0077	7.27	0.065
2484.18	Sil		0.0093	0.0081	6.47	0.049
2485.15	cMl		0.0093	0.0075	7.82	0.052
2487.16	cMl		0.0101	0.0084	7.33	0.064
2650.38	cMl		0.0060	0.0062	5.47	0.021
2651.75	Sim		0.0078	0.0069	6.58	0.029
2651.92	Sim		0.0078	0.0067	6.96	0.032
2652.62	Sim		0.0085	0.0075	6.28	0.035
2653.45	Sim		0.0093	0.0071	6.31	0.032
2654.24	Sim		0.0131	0.0094	5.93	0.064
2664.35	cMl		0.0078	0.0069	6.23	0.028
2666.40	mH		0.0078	0.0074	5.60	0.034

Table 3: Summary of results from MICP analysis.

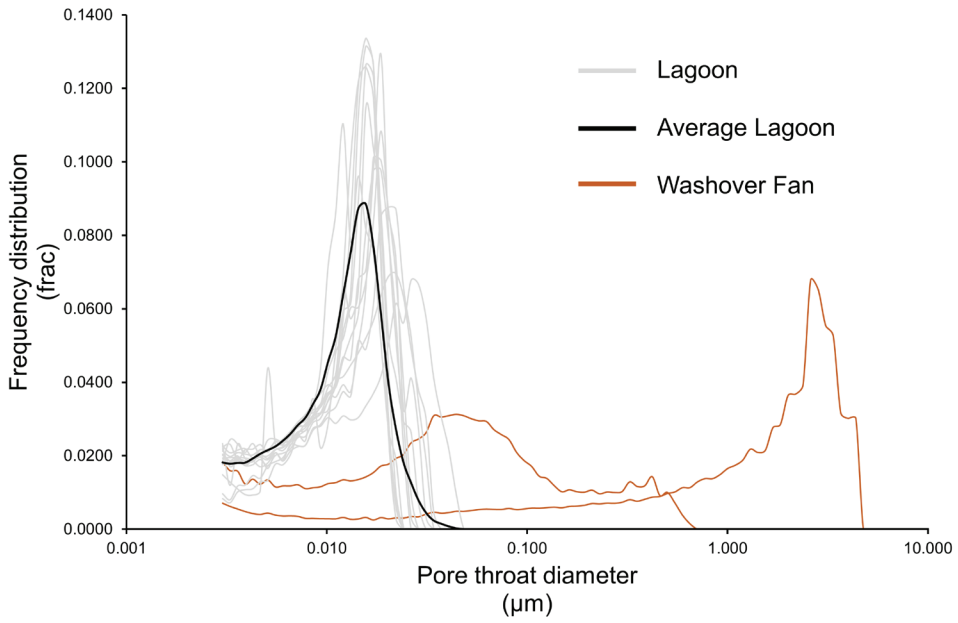

Figure 13: Comparison of pore size distributions obtained through the MICP analysis. The bold black curve represents the mean of all Lagoon samples.

succession of up to 2 m thick. Overall, the bioturbation intensity is moderate. Trace fossils assemblage dominantly includes *Planolites* with *Thalassinoides, Palaeophycus, Skolithos, Teichichnus*, and *Scolicia.*

Interpretation: Dominance of fine-grained sediments suggests deposition in an overall low energy setting. The local presence of structureless sandstone indicates pulses of high rates of sediment fallout. Presence of climbing ripples, which record both lateral migration and vertical aggradation of the bedform, indicate sub-environments with high rates of deposition from decelerating flows. High suspension loads could stem from floodwaters breaking from the channel margin and spreading across an adjacent floodplain. Furthermore, the lenticular bedding suggests that the proportion of mud in these beds is likely equal to or greater than the proportion of sand. In addition, localized syneresis cracks are formed due to change in salinity in the pore water of muddy sediments (Pratt, 1998). The trace fossil suite, comprising horizontal grazing trails and feeding trails, with the vertical dwelling structures, suggests that these deposits became interbedded with marginal-marine strata displaying ichnological evidence of brackish-water influence. These deposits could also be representing backbarrier deposits (Hayes and FitzGerald, 2013).

4.2. Mineralogy and MICP

Based on the macro- and microscale features of the identified depositional facies, as described in the preceding section, the lagoon deposits appear to be the most abundant and relevant sealing facies. In order to evaluate their sealing potential, additional analysis was conducted on selected samples (n=14) from the lagoon facies. These samples captured not only the range of lithofacies observed within the lagoon deposits but also the depth variation, as the lagoon deposits occur at different stratigraphic levels (Figs. 5 and 6). In addition, two samples from the washover fan facies were analyzed.

The mineralogy is obtained primarily from XRD analysis, complemented with optical microscope observation and mineral maps created through QEMSCAN analysis in order to understand any preferential distribution of the minerals. XRD data reveals that the lagoonal deposits consist primarily of quartz, K-feldspar, plagioclase, calcite, dolomite, ankerite, siderite, and pyrite in varying proportions. Total carbonate minerals content varies between 14 and 42 wt%, whilst detrital minerals such as quartz and feldspars fall within the 24–37 wt% range (Fig. 11). It is interesting to note that the laminated siltstones contain relatively higher carbonate minerals than the other lithofacies. QEMSCAN analysis suggested presence of carbonate cements, primarily calcite, along the lamination. Calcite is also partly present in the form of microfossils.

Total clay content is significantly higher, as expected, and varies between 34 and 55 % (Fig. 11). The clay minerals identified among these samples include illite, kaolinite, chlorite and smectite, with illite being the most dominant type, followed by smectite (Fig. 12a, b; Tab. 2). Furthermore, kaolinite and chlorite contents are relatively low. However, no preferential mode of distribution for the clay minerals is evident in the minerals maps created from the subset of 7 samples. QEMSCAN analysis also highlighted the presence of scarce, scattered heavy minerals (e.g., 2481.21 m), mostly garnet. The abundance of smectite recorded on the selected samples of the lagoon facies displays an interesting trend: the deeper samples from 2650–2666 m (Fig. 12b), irrespective of their lithofacies, have lower smectite content than their shallower counterparts from 2481–2487 m (Fig. 12a). The two additional samples belonging to washover fan facies from 2655–2657 m depth also contain negligible amounts of smectite (Tab. 2).

The MICP results are listed in Table 3 and displayed in terms of mean pore throat size in Figure 13. The result from this study is akin to Skerbisch et al. (2023), who published MICP data from selected mudstones across the Vienna Basin to establish a basin-wide compaction trend based on theoretical models, and then compared it with the theoretical maximum hydrocarbon column heights inferred from true measured capillary pressure curves.

Most of the results are from the lagoon facies, where porosity values range between 5 and 8 %, whilst permeabilities are in nD range. The pore-throat diameter (D50) ranges between 0.006 µm and 0.009 µm, with an overall mean value of 0.007 µm. It is interesting to note that the mode and D50 values are very similar, suggesting 'unimodal' pore sizes. However, among washover fan samples, there is indication of multimodal pore sizes related to sorting of grains (Fig. 12a, b). Note that these two samples belong to Sm and mH lithofacies.

4.3. CoreDNA Analysis

Suitable cores from two widely separated intervals of the lagoon facies, namely 2480–2484 m (Fig. 14) and 2676–2685 m (Fig. 15), were analysed on CoreDNA test series. These selected intervals, however, could not be tested continuously due to the broken nature of the cores (broken into discs). Richard et al. (2012) provided compelling experimental evidence that the unconfined compressive strength (UCS) of rocks can be reliably assessed from scratch tests performed under controlled conditions. These include utilising a sharp cutter and depth of cut small enough to assure that cutting takes place in the ductile regime. This technique yields a continuous log of the rock strength and the spatial variation of the strength, which in turns provides not only valuable insights on the inhomogeneity of the rock but also a context to the conventional meaning of the UCS.

The unconfined compressive strength of Lagoon deposits varies between 29 and 104 MPa. However, a subtle difference can be observed between the two sections in terms of rock strength, where it is slightly higher (P50 = 62 MPa) in the deeper section (Fig. 15) in relation to the

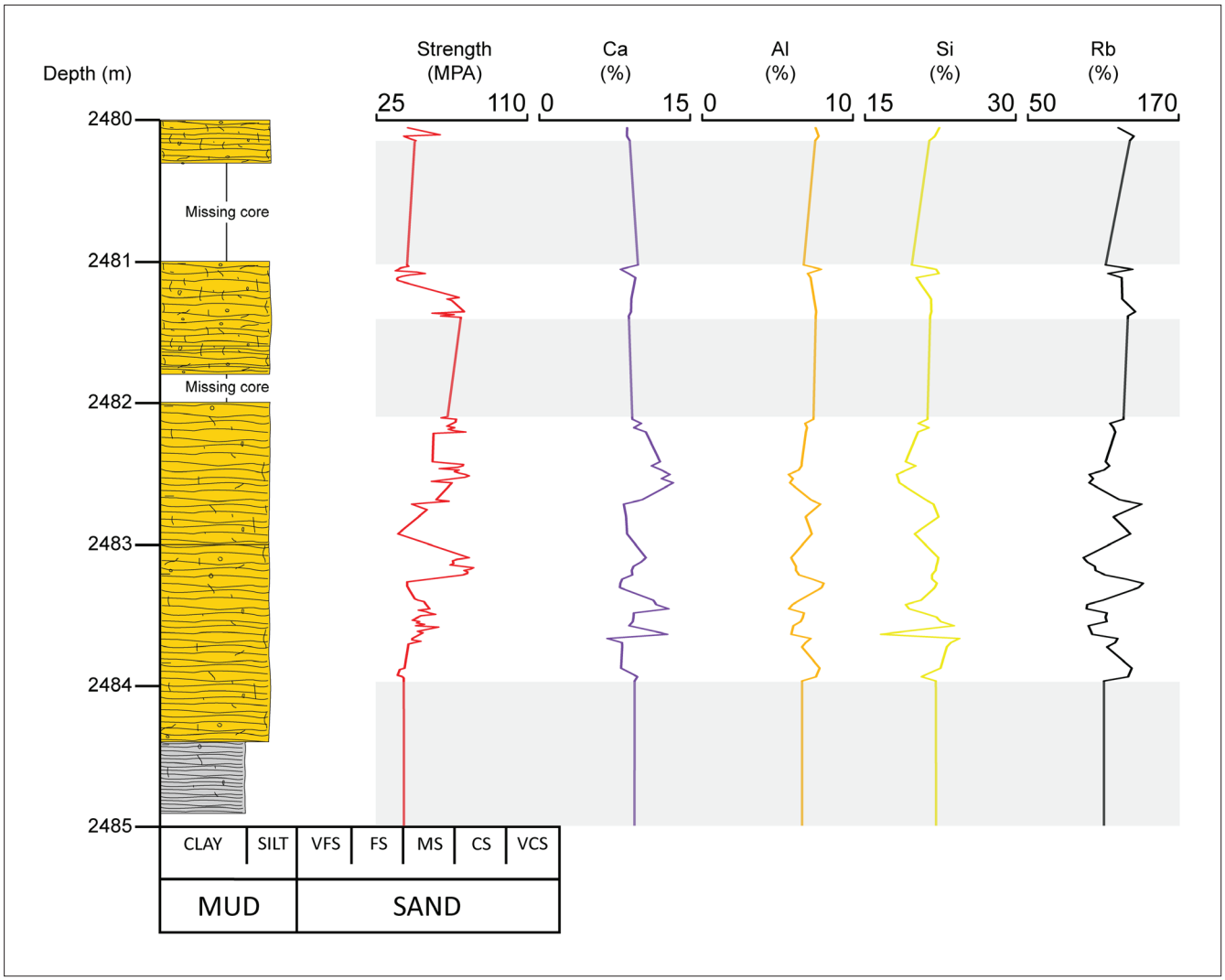

Figure 14: Rock strength and elemental composition of the shallower Lagoon facies (Cf. Fig. 6). Data collected through coreDNA analysis. Grey shaded intervals have no data points. The two lagoon intervals (Cf. Figs. 5 and 6) are separated by 190 m vertically.

shallower section (P50 = 56 MPa) (Fig. 14). The coreDNA dataset also highlighted that these slight changes in strength are likely due to the higher abundance of clay, as suggested by the concentrations of Al, Rb, and Si (Fig. 14). In addition, high Ca concentrations in the shallower section (Fig. 14) are reflecting higher calcite and/or Ca-rich smectite contents.

5. Discussion

5.1. Depositional model

The facies associations interpreted in the current study from the cores predominantly suggested a coastal lagoon environment prevailed in the location of the well. Coastal lagoons are shallow inland water bodies, occurring in topographic depressions that are separated from the sea/ocean by narrow barriers (Kjerfve, 1994; Clifton, 2005). They are connected to the sea/ocean by one or more channels, known as inlets, which often cuts through a narrow barrier island of erodible material and remain open at least intermittently. Water exchange occurs between the lagoon and the sea because of tides, river flow, wind, and waves (Hayes and FitzGerald, 2013). The short-lived stages of connection alternate with periods of restriction, dictating the recorded environmental conditions. They are also affected by frequent changes in sea-level, tidal currents, hydrological regimes, salinity, nutrient supply and continental runoff, or sedimentary dynamics (Hewins and Perry, 2006; Vidal et al., 2007; Pereira Coutinho et al., 2012). Coastal lagoons are therefore very specific and highly dynamic environments and hold special interest as sedimentary archives. Harzhauser et al (2020), based on the faunal assemblages interpreted, that the sedimentation of the Bockfließ Fm occurred in a lagoonal-coastal depositional environment, with mudflats and soft bottom conditions in a fully marine environment. Furthermore, the sedimentary facies analysis in the current study also pointed out the presence of channel-fills, washover fan and shoreface deposits in this location. The channel deposits and associated facies

recognised in this study could represent inlets to the lagoon.

There are two main modes of coastal lagoon formation: inundation model and spit-embayment model (Gilbert, 1885; McGee, 1890). In the spit-embayment model (Gilbert, 1885), littoral processes build sand bodies seaward of a previously smoothed and straightened coastline. Spits are generally narrow, low-profile sand bodies that are subject to overwash during storms. During overwash, sand is dispersed landward across the spit and deposited in fans. Multiple washover fans often coalesce along the back barrier forming a wavy or scalloped shore. This type of lagoon formation is probable along wave-dominated coasts with regressive seas or very slow shifts in sea level.

As per the inundation model of formation (McGee, 1890), lagoons form when basins are flooded by the coastal sea and a small conduit is maintained that allows a free exchange of water between the lagoon and the sea. Coastal lagoons in flooded drainage basins inherit the shapes of the basin contours and generally produce triangular or delta-shaped water bodies with coast-parallel seaward margins and V-shaped landward margins. With prolonged sea-level rise, inundation may submerge the interfluve between two adjacent basins causing adjacent delta bays to coalesce (Clifton, 2005).

In case of the current study, the inundation model seems probable given that Harzhauser et al. (2020) concluded, based on correlation of the Bockfließ Fm with the Lužice Fm, that the Bockfließ Fm represents a transgressive systems tract and early high stand systems tract of the 3rd order TB 2.1. cycle of Haq et al. (1988), which agrees with Piller et al. (2007). The vertical association of facies interpreted from the cores in Matzen 269 suggest juxtaposition of shallow marine (inlets) deposits on top of lagoon deposits. This corroborates the findings from previous studies in terms of sequence stratigraphy (Haq et al., 1988; Piller et al., 2007). It is noteworthy that the cores only represent roughly one quarter of the total Bockfließ Fm thickness in the studied location, and other facies associated with coastal lagoons such as barrier island system has not been captured by the cores.

5.2. Modern analogue

Modern coastal lagoons present a great variety of dimensions, from 10000 m^2 to 10000 km^2. The largest in the Mediterranean Sea is the Venice Lagoon (~550 km^2; mean depth 1.1 m), which is a shallow microtidal basin defined by a complex network of channels and intertidal flats forming a major salt marsh complex (Kaniewski et al., 2024). In the Baltic Sea the largest is the Curonian lagoon. It is located in the south-eastern part of the Baltic Sea with a total surface of 1584 km^2 and average depth of 3.8 m (Magri et al., 2024). This microtidal lagoon is connected to the Baltic Sea by a narrow, 11 km long strait (0.4–1.1 km wide, 8–15 m deep). On the other hand, Chilika Lake on the east coast of India, representing Asia's largest brackish water lagoon, is pear-shaped and has an average depth of about 1.4 m covering a total area of nearly 750 km^2 in the dry season that extends up to about 1100 km^2 during the rainy season (Bhuvanagiri et al., 2018). The Lagoa dos Patos lagoon, located in the coastal plain of Rio Grande do Sul State, South Brazil, is ~240 km long and ~40 km wide, with an average depth of ~6 m. It covers an area ~10000 km^2 (Lopes et al., 2022).

Based on a single well, interpreting the lateral changes of the facies identified in cores, hence the dimension of the lagoon, is a formidable task and fraught with high uncertainties. However, the Bockfließ Fm has been documented from several subsurface drillings in the Central Vienna Basin (Harzhauser et al., 2020). A continuation in eastern direction into the Gajary depression on Slovak territory was described by Kováč et al. (2004). Its western boundary is marked by Aderklaa High and Aderklaa-Bockfließ Fault, whilst in southern direction, the Bockfließ Fm pinches out in the Gänserndorf area (Harzhauser et al., 2020). Based on this, it could be deduced that the coastal lagoon identified in this study could measure 10 s of km in the widest stretch.

5.3. Sealing potential

The sealing potential of a caprock system could be defined as the geometry, capacity and integrity of the caprock (Kaldi and Atkinson, 1997). Seal geometry refers to the structural position, thickness and lateral extent of the caprock. These can be estimated by integrated studies of seismic, well and core data through geological/depositional models. The seal capacity refers to the maximum fluid column height that can be retained in the underlying reservoir before pressure exerted by buoyancy exceeds capillary entry pressure. The seal capacity is typically determined via analytical methods (mercury intrusion capillary pressure; MICP). Finally, the seal integrity is controlled by the geomechanical properties in the context of ambient stress fields that may be modified by fluid withdrawal/injection. It is interesting to note that the caprock thickness does not influence the capillary entry pressure but is critical for continuity in faulted regimes.

The *seal geometry* has been discussed in terms of the depositional model of the lagoon. Additionally, given the vertical juxtaposition of facies, it is assumed that the lagoon deposits would most likely act as an intraformational seal given that Bockfließ Fm also contains other non-sealing deposits such as washover fan sandstones or heterolithics (Fig. 4; Table 1). The actual proportion of lagoon facies is difficult to quantify as the core coverage in the study well is *c.*28 % of the total formation thickness (Fig. 4). However, within the cored interval the lagoon deposits represent 46 % of the cored thickness (Fig. 4). The basal part of the formation comprises calcareous shoreface sandstones that could also act as a barrier.

The *seal capacity* of a rock is controlled by pore throat size, contact angle (wettability), and interfacial tension (IFT) such that the column height (capillary pressure) of fluids in a reservoir increases as 1) pore throat size in the

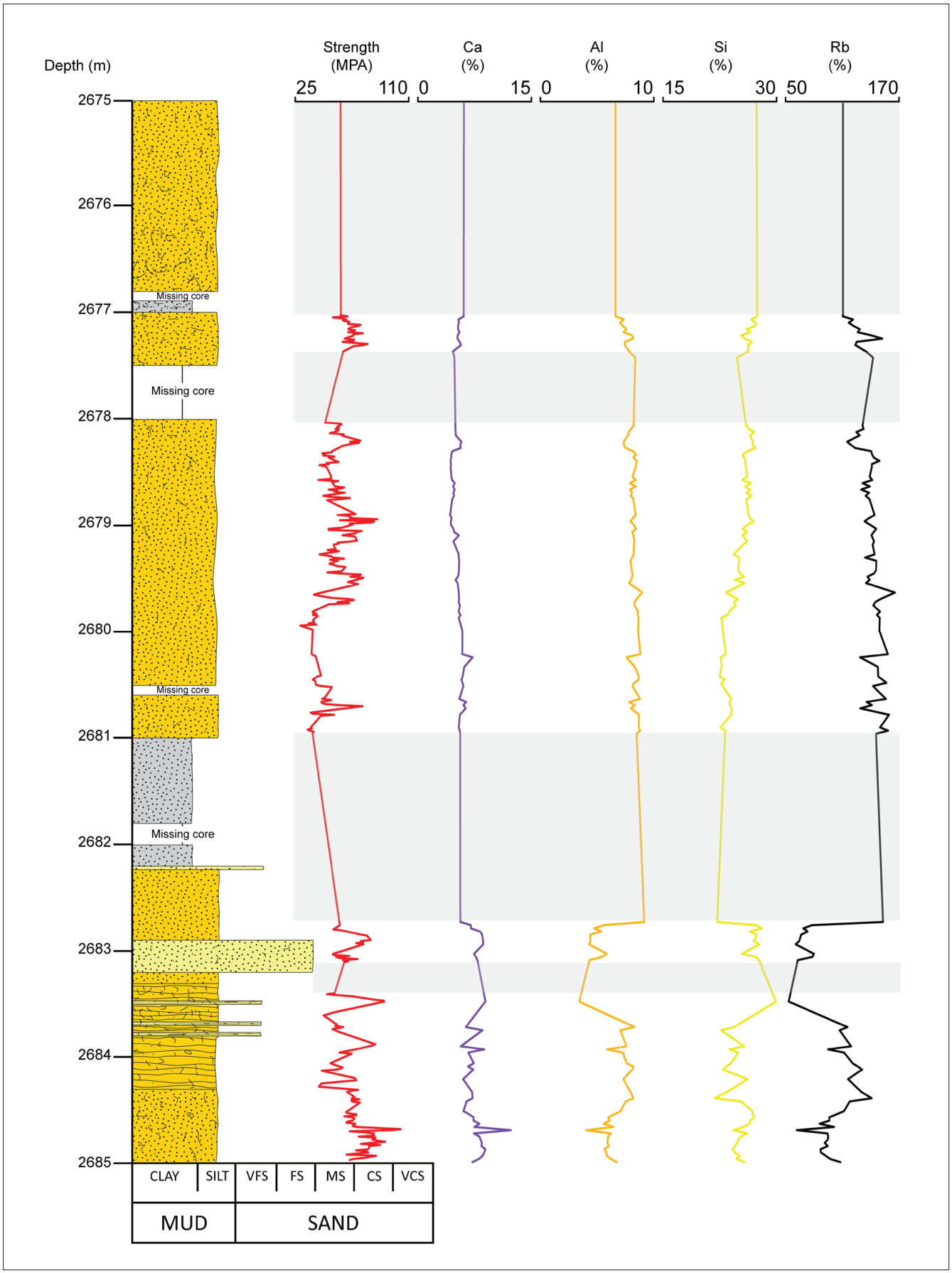

Figure 15: Rock strength and elemental composition of the deeper Lagoon facies (Cf. Fig. 5). Data collected through coreDNA analysis. Grey shaded intervals have no data points. The two lagoon intervals (Cf. Figs. 5 and 6) are separated by 190 m vertically.

seal decreases; 2) the wettability between the hydrocarbon-water-rock or gas-water-rock system decreases; and 3) the IFT between hydrocarbons or other gas and water increases (Daniel and Kaldi, 2009). The MICP data (Table 3) from this study could be used to assess the column height of fluid that the lagoon facies can hold before it leaks.

The caprock geomechanical property, or the *seal integrity*, in this study is represented by the unconfined compressive strengths measured as part of the coreDNA analysis (Figs. 14 and 15). These limited data suggest a subtle change of strength within the lagoon facies, owing to the clay content (Fig. 11). Bourg (2015) conducted a series of experiments and found that clay mineral mass fraction, Xclay, controls key material properties of fine-grained rocks and that a remarkably sharp threshold at Xclay ~1/3 separates them with very different properties. For example, the unconfined compressive strength decreases by a factor of 20 at Xclay >33 %, vertical permeability decreases considerably by a factor of 6 when Xclay = 0–35 % and further by 1.5 factor when it is 35–70 %. The porosity values also change considerably at Xclay >33 %, which indicate significant increase of sensitivity of porosity to maximum burial depth, cementation and recrystallization. These findings indicate a strong relationship between rock properties and clay content, specifically the threshold of Xclay ~33 % is crucial in assessing seal capacity of mudrocks (Bourg, 2015) (Fig. 11). The selected samples from the lagoon facies in Matzen 269 represent the 'sealing shales' sensu Bourg (2015). Interestingly, shales and mudstones below the Xclay ~1/3 have good reservoir qualities and are exploited for hydrocarbons, whereas shales and mudstones above the Xclay ~1/3 threshold are utilized or considered for CCS and radioactive waste storage (Bourg, 2015).

The dominant clay species across the lagoon facies is illite (Fig. 12a, b; Tab. 2), which is considered non-reactive (Busch et al., 2016; Worden, 2023). Reactive clay species abundance, like smectite, is significant among the shallower section of the formation in the study well, where possibility of contact between the reservoir fluid and the caprock is minimal. Interestingly, depending on the type of fluid, smectite-rich mudstone either lead to dehydration cracks that can provide pathways for fluid migration or to swelling improving seal integrity by the closure of fractures or the reduction of fracture apertures (Busch et al., 2016).

6. Conclusions

The Lower Miocene Bockfließ Formation in the Central Vienna Basin has its type section in the subsurface well Matzen 269. Around 28 % of the formation's thickness has been captured by several historical subsurface cores, collected as part of classic E&P projects. These cores were subjected to various analyses, including sedimentology, petrography, XRD, QEMSCAN, MICP, and coreDNA, for a detailed and holistic characterization of the formation. These analyses provided a holistic dataset covering the sedimentological, petrophysical, and geomechanical aspects of the formation for the first time. The detailed sedimentological characterization suggests that the Bockfließ Fm at this location largely represents a coastal lagoon depositional setting, with depositional environments such as lagoon, washover fan, channel-fills, channel-margins and shoreface identified. The identified lagoon could span tens of kilometres at its widest point and most likely formed due to coastal sea flooding. However, a connection was maintained between the lagoon and the sea, representing an inundation model.

The fine-grained sediment of the extensive lagoon facies facilitated its role as a regional caprock for the underlying fractured carbonate reservoirs containing hydrocarbons. In the context of sealing potential, the lagoon facies would most likely act as an intraformational seal, as the Bockfließ Fm also contains other non-sealing facies. MICP-derived data has also corroborated this notion. Rock strength data obtained through scratch testing indicate a subtle variation in strength within the lagoon facies, attributed to clay content. Based on XRD data, the selected samples from the lagoon facies in Matzen 269 represent 'sealing shales' in the sense described by Bourg (2015). It is noteworthy that rock-fluid interactions may alter the caprock properties, however, illite is identified as the dominant clay mineral across the lagoon facies, which is considered non-reactive.

Acknowledgements

Yaroslav Zechner greatly acknowledges colleagues from the Core & Cuttings Technologies Department, OMV for technical support and constructive discussions during his internship, namely A. Vršič, T. Kuffner, A. Metz, E. Mekonnen and W. Hujer. Viridien UK is acknowledged for undertaking QEMSCAN analysis on our behalf. Additionally, we thank OMV Energy Tech Center management for permitting us to publish this article. We are grateful to reviewers M. Harzhauser (NHM, Vienna) and S. Gier (University Vienna), Associate Editor M. Bestmann, and Chief Editor K. Stüwe for their careful reviews and constructive comments to improve this work.

References

Allen J.R.L., 1983. Studies in fluviatile sedimentation: Bars, bar-complexes and sandstone sheets (low-sinuosity braided streams) in the brownstones (L. devonian), welsh borders. Sedimentary Geology 33/4, 237–293. https://doi.org/10.1016/0037-0738(83)90076-3.

Bhuvanagiri S.R.V.P., Pichika S., Akkur R., Chaganti K., Madhusoodhanan R., Pusapati S.V., 2018. Integrated Approach for Modeling Coastal Lagoons: A Case for Chilka Lake, India, in: Srinivasa Rao, A.S.R., Rao, C.R. (Eds.), Integrated Population Biology and Modeling, Part A, vol. 39. Elsevier, 343–402. https://doi.org/10.1016/bs.host.2018.06.005.

Bourg I.C., 2015. Sealing Shales versus Brittle Shales: A Sharp Threshold in the Material Properties and Energy Technology Uses of Fine-Grained Sedimentary Rocks. Environ. Sci. Technol. Lett. 2/10, 255–259. https://doi.org/10.1021/acs.estlett.5b00233.

Bridge J.S., 2006. Fluvial Facies Models: Recent Developments, in:

Posamentier, H.W. (Ed.), Facies models revisited. Society for Sedimentary Geology, Tulsa, Okla., 85–170. https://doi.org/10.2110/pec.06.84.0085.

Busch A., Bertier P., Gensterblum Y., Rother G., Spiers C.J., Zhang M., Wentinck H.M., 2016. On sorption and swelling of CO2 in clays. Geomech. Geophys. Geo-energ. Geo-resour. 2/2, 111–130. https://doi.org/10.1007/s40948-016-0024-4.

Clifton H.E., 2005. Coastal Sedimentary Facies, in: Schwartz, M.L. (Ed.), Encyclopedia of Coastal Science. Springer Netherlands, Dordrecht, 270–278. https://doi.org/10.1007/1-4020-3880-1_84.

Daniel R.F., Kaldi J.G., 2009. Evaluating Seal Capacity of Cap Rocks and Intraformational Barriers for CO2 Containment, in: Grobe, M., Pashin, J.C., Dodge, R.L. (Eds.), Carbon Dioxide Sequestration in Geological Media-State of the Science, vol. 59. American Association of Petroleum Geologists, 335–345. https://doi.org/10.1306/St591317.

Decker K., 1996. Miocene tectonics at the Alpine-Carpathian junction and the evolution of the Vienna Basin. Mitt Ges Geol Bergbaustud Österr 41, 33–44. https://opac.geologie.ac.at/ais312/dokumente/Mitteilungen_Band41_A.pdf.

Dickson J.A.D., 1965. A Modified Staining Technique for Carbonates in Thin Section. Nature 205/4971, 587. https://doi.org/10.1038/205587a0.

Germay C., Lhomme T., Perneder L., 2023. High-resolution core data and machine learning schemes applied to rock facies classification. SP 527/1, 121–135. https://doi.org/10.1144/SP527-2021-193.

Gilbert G.K., 1885. The topographic features of lake shores. US Government Printing Office. https://doi.org/10.1038/034269a0.

Hamilton W., Wagner L., Wessely G., 2000. Oil and Gas in Austria. Mitt. Österr. Geol. Ges. 92, 235–262. https://www.geologie.or.at/images/OEGG/geol-ges/mitteilungen/mitt-92.html.

Haq B.U., Hardenbol J.A.N., Vail P.R., 1988. Mesozoic and Cenozoic chronostratigraphy and cycles of sea-level change, in: Wilgus C.K., Hastings B.S., Posamentier H., van Wagoner J., Ross C.A., St. Kendall C.G.C. (Eds.), Sea-Level Changes. SEPM (Society for Sedimentary Geology), 71–108. https://doi.org/10.2110/pec.88.01.

Harzhauser M., Kranner M., Mandic O., Strauss P., Siedl W., Piller W.E., 2020. Miocene lithostratigraphy of the northern and central Vienna Basin (Austria). Austrian Journal of Earth Sciences 113/2, 169–199. https://doi.org/10.17738/ajes.2020.0011.

Harzhauser M., 2022. Vienna Basin, Korneuburg Basin. In: Piller W.E. (Ed.), Friebe J.G., Gross, M., Harzhauser M., Van Husen D., Koukal V., Krenmayr H.G., Krois P., Nebelsick J.H., Ortner H., Piller W.E., Reitner J.M., Roetzel R., Rögl F., Rupp C., Stingl V., Wagner L., Wagreich M., 2022. Stratigraphic Chart of Austria – Cenozoic. Abhandlungen der Geologische Bundesanstalt, 76, 163–181. https://www.inatura.at/forschung-online/piller_etal_2022_lithounits_cenozoic_austria_abh-gba_76.pdf.

Harzhauser M., Kranner M., Siedl W., Conradi F., Piller W.E., 2024a. The Neogene of the Vienna Basin – a synthesis. In: Tari G. C., Kitchka A., Krézsek C., Lučić D., Markič M., Radivojević D., Sachsenhofer R.F., Šujan M. (eds) The Miocene Extensional Pannonian Superbasin, Volume 1: Regional Geology. Geological Society, London, Special Publications, 554. https://doi.org/10.1144/SP554-2023-168.

Harzhauser M., Landau B., Mandic O., Neubauer T.A., 2024b. The Central Paratethys Sea-rise and demise of a Miocene European marine biodiversity hotspot. Scientific Reports, 14, 16288, 2024. https://doi.org/10.1038/s41598-024-67370-6.

Hayes M., FitzGerald D., 2013. Origin, Evolution, and Classification of Tidal Inlets. Journal of Coastal Research, 69, 14–33. https://doi.org/10.2112/SI_69_3.

Hewins M.R., Perry C.T., 2006. Bathymetric and Environmentally Influenced Patterns of Carbonate Sediment Accumulation in Three Contrasting Reef Settings, Danjugan Island, Philippines. Journal of Coastal Research 224, 812–824. https://doi.org/10.2112/04-0158.1.

Hölzel M., Decker K., Zámolyi A., Strauss P., Wagreich M., 2010. Lower Miocene structural evolution of the central Vienna Basin (Austria). Marine and Petroleum Geology 27/3, 666–681. https://doi.org/10.1016/j.marpetgeo.2009.10.005.

Kaldi J.G., Atkinson C.D., 1997. Evaluating Seal Potential Example from the Talang Akar Formation, offshore Northwest Java, Indonesia. In: Surdam, R.C. (Ed.), Seals, Traps, and the Petroleum System. American Association of Petroleum Geologists. https://doi.org/10.1306/M67611.

Kaniewski D., Marriner N., Vacchi M., Camuffo D., Bivolaru A., Sarti G., Bertoni D., Diatta L., Markakis N., Martella A., Otto T., Luce F., Calaon D., Cottica D., Morhange C., 2024. Holocene Sea-level impacts on Venice Lagoon's coastal wetlands. Global and Planetary Change 236, 104426. https://doi.org/10.1016/j.gloplacha.2024.104426.

Kjerfve B., 1994. Chapter 1 Coastal Lagoons, in: Coastal Lagoon Processes, vol. 60. Elsevier, pp. 1–8. https://doi.org/10.1016/S0422-9894(08)70006-0.

Kováč M., Baráth I., Harzhauser M., Hlavatý I., Hudackova N., 2004. Miocene depositional systems and sequence stratigraphy of the Vienna Basin. CFS Courier Forschungsinstitut Senckenberg 246, 187–212.

Lopes C.T., Savian J.F., Frigo E., Endrizzi G., Hartmann G.A., Santos N.O., Trindade R.I.F., Ivanoff M.D., Toldo E.E., Fauth G., Oliveira L.V., Bom M.H.H., 2022. Late Holocene paleosecular variation and relative paleointensity records from Lagoa dos Patos (southern Brazil). Physics of the Earth and Planetary Interiors 332, 106935. https://doi.org/10.1016/j.pepi.2022.106935.

MacEachern J.A., Bann K.L., Gingras M.K., Zonneveld J.-P., Dashtgard S.E., Pemberton S.G., 2012. The Ichnofacies Paradigm, in: Knaust, D., Bromley, R.G. (Eds.), Trace Fossils as Indicators of Sedimentary Environments, vol. 64. Elsevier, 103–138. https://doi.org/10.1016/B978-0-444-53813-0.00004-6.

Magri M., Bondavalli C., Bartoli M., Benelli S., Žilius M., Petkuviene J., Vybernaite-Lubiene I., Vaičiūtė D., Grinienė E., Zemlys P., Morkūnė R., Daunys D., Solovjova S., Bučas M., Gasiūnaitė Z.R., Baziukas-Razinkovas A., Bodini A., 2024. Temporal and spatial differences in nitrogen and phosphorus biogeochemistry and ecosystem functioning of a hypertrophic lagoon (Curonian Lagoon, SE Baltic Sea) revealed via Ecological Network Analysis. The Science of the total environment 921, 171070. https://doi.org/10.1016/j.scitotenv.2024.171070.

McGee W.J., 1890. The southern extension of the Appomattox Formation. American Journal of Science 3/235, 15–41. https://doi.org/10.2475/ajs.s3-40.235.15.

McRae S.G., 1972. Glauconite. Earth-Science Reviews 8/4, 397–440. https://doi.org/10.1016/0012-8252(72)90063-3.

Miall A.D., 2006. The Geology of Fluvial Deposits. Springer Berlin Heidelberg, Berlin, Heidelberg. https://doi.org/10.1007/978-3-662-03237-4.

Morsilli M., Pomar L., 2012. Internal waves vs. surface storm waves: a review on the origin of hummocky cross-stratification. Terra Nova 24/4, 273–282. https://doi.org/10.1111/j.1365-3121.2012.01070.x.

Neubauer T.A., Harzhauser M., Kroh A., Georgopoulou E., Mandic O., 2015. A gastropod-based biogeographic scheme for the European Neogene freshwater systems. Earth-Science Reviews 143, 98–116. https://doi.org/10.1016/j.earscirev.2015.01.010.

Papp A., Krobot W., Hladecek K., 1973. Zur Gliederung des Neogens im Zentralen Wiener Becken. Mitt. Ges. Geol. Berbaustud, Band 22, 191–199. https://opac.geologie.ac.at/ais312/dokumente/Mitteilungen_Band22_A.pdf.

Pemberton S.G., MacEachern J.A., Dashtgard S.E., Bann K.L., Gingras M.K., Zonneveld J.-P., 2012. Shorefaces, in: Knaust D., Bromley R.G. (Eds.), Trace Fossils as Indicators of Sedimentary Environments, vol. 64. Elsevier, 563–603. https://doi.org/10.1016/B978-0-444-53813-0.00019-8.

Pereira Coutinho M.T., Brito A.C., Pereira P., Gonçalves A.S., Moita M.T., 2012. A phytoplankton tool for water quality assessment in semi-enclosed coastal lagoons: Open vs closed regimes. Estuarine, Coastal and Shelf Science 110, 134–146. https://doi.org/10.1016/j.ecss.2012.04.007.

Piller W.E., Harzhauser M., Mandic O., 2007. Miocene Central Paratethys stratigraphy – current status and future directions. strat 4/2–3, 151–168. https://doi.org/10.29041/strat.04.2.09.

Popov S.V., Rögl F., Rozanov A.Y., Steininger F.F., Shcherba I.G., and Kováč M., 2004. Lithological-Paleogeographic maps of the Paratethys. 10 maps Late Eocene to Pliocene. Courier Forsch.-Inst. Senckenberg 250, 1–46.

Pratt B.R., 1998. Syneresis cracks: subaqueous shrinkage in argilla-

ceous sediments caused by earthquake-induced dewatering. Sedimentary Geology 117/1–2, 1–10. https://doi.org/10.1016/S0037-0738(98)00023-2.
Reineck H.-E., Singh I.B., 1973. Depositional Sedimentary Environments. Springer Berlin Heidelberg, Berlin, Heidelberg. https://doi.org/10.1007/978-3-642-81498-3.
Richard T., Dagrain F., Poyol E., Detournay E., 2012. Rock strength determination from scratch tests. Engineering Geology 147–148, 91–100. https://doi.org/10.1016/j.enggeo.2012.07.011.
Rubio B., López-Pérez A.E., 2024. Exploring the Genesis of Glaucony and Verdine Facies for Paleoenvironmental Interpretation: A review. Sedimentary Geology. 461. 106579. https://doi.org/10.1016/j.sedgeo.2024.106579.
Ruman A., Ćorić S., Halásová E., Harzhauser M., Hudáčková N., Jamrich M., Palzer-Khomenko M., Kranner M., Mandic O., Radionova E.P., Rybár S., Šimo V., Šujan M., Kováč M., 2021. The "Rzehakia beds" on the northern shelf of the Pannonian Basin: biostratigraphic and palaeoenvironmental implications. Facies 67/1. https://link.springer.com/article/10.1007/s10347-020-00609-6.
Sachsenhofer R.F., Misch D., Rainer T., Rupprecht B.J., Siedl W., 2024. The Vienna Basin: petroleum systems, storage and geothermal potential. Geological Society, London, Special Publications, 555, SP555-2023-205. https://doi.org/10.1144/SP555-2023-205.
Schultz L.G., 1964. Quantitative interpretation of mineralogical composition from X-ray and chemical data for the Pierre Shale. Professional Paper 391C. https://pubs.usgs.gov/publication/pp391C.
Schultz O., 2005. Catalogus fossilium Austriae. Verl. der Österr. Akad. der Wiss, Wien, 6911212 pp. https://doi.org/10.1553/0x000d1cf8.
Siedl W., Strauss P., Sachsenhofer R.F., Harzhauser M., Kuffner T., Kranner M., 2020. Revised Badenian (middle Miocene) depositional systems of the Austrian Vienna Basin based on a new sequence stratigraphic framework. Austrian Journal of Earth Sciences 113/1, 87–110. https://doi.org/10.17738/ajes.2020.0006.
Skerbisch L., Misch D., Drews M., 2023. Regional mudstone compaction trends in the Vienna Basin: top seal assessment and implications for uplift history. Int J Earth Sci (Geol Rundsch) 112, 1901–1921. https://doi.org/10.1007/s00531-023-02331-4.
Strauss P., Harzhauser M., Hinsch R., Wagreich M., 2006. Sequence stratigraphy in a classic pull-apart basin (Neogene, Vienna Basin). A 3D seismic based integrated approach. Geologica Carpathica 57. http://www.scopus.com/scopus/inward/record.url?eid=2-s2.0-33746562405&partner@&rel=R5.0.4.
Surdam R.C., 1997. Seals, Traps, and the Petroleum System. American Association of Petroleum Geologists. https://doi.org/10.1306/M67611.
Talman S.G., Keough M.J., 2001. Impact of an exotic clam, Corbula gibba, on the commercial scallop Pecten fumatus in Port Phillip Bay, south-east Australia: evidence of resource-restricted growth in a subtidal environment. Marine Ecology Progress Series 221, 135–143. https://doi.org/10.3354/meps221135.
Thomeer J., Murphy D., 2000. Capillarity in rocks. Shell/OGCI PetroSkills.
Tucker M.E., Jones S., 2023. Sedimentary petrology. Wiley, Hoboken, NJ, 426 pp. ISBN: 9781118786499
Vidal L., Rodríguez-Gallego L., Conde D., Martínez-López W., Bonilla S., 2007. Biomass of autotrophic picoplankton in subtropical coastal lagoons: Is it relevant? Limnetica 26/2, 441–452. https://doi.org/10.23818/limn.26.37.
Worden R.H., 2023. Value of core for reservoir and top-seal analysis for carbon capture and storage projects. Geological Society, London, Special Publications, Volume 527, 365–385. https://doi.org/10.1144/SP527-2022-38.

Received: 30.4.2025
Accepted: 3.8.2025
Editorial Handling: Michel Bestmann